Transferable potential function for flexible H2O molecules based on the single-center multipole expansion

Jónsson, E.Ö.; Rasti, R.; Galynska, M.; Meyer, J.; Jónsson, H.

JCTC Journal of Chemical Theory and Computation

pubs.acs.org/JCTC Article

Transferable Potential Function for Flexible H_2O Molecules Based on the Single-Center Multipole Expansion

Elvar Örn Jónsson,* Soroush Rasti, Marta Galynska, Jörg Meyer, and Hannes Jónsson

Cite This: J. Chem. Theory Comput. 2022, 18, 7528−7543 Read Online

ACCESS | Metrics & More | Article Recommendations | Supporting Information

ABSTRACT: A potential function is presented for describing a system of flexible H_2O molecules based on the single-center multipole expansion (SCME) of the electrostatic interaction. The model, referred to as SCME/f, includes the variation of the molecular quadrupole moment as well as the dipole moment with changes in bond length and angle so as to reproduce results of high-level electronic structure calculations. The multipole expansion also includes fixed octupole and hexadecapole moments, as well as anisotropic dipole−dipole, dipole−quadrupole, and quadrupole−quadrupole polarizability tensors. The model contains five adjustable parameters related to the repulsive interaction and damping functions in the electrostatic and dispersion interactions. Their values are adjusted to reproduce the lowest energy isomers of small clusters, $(H_2O)_n$ with n = 2−6, as well as measured properties of the ice Ih crystal. Subsequent calculations of the energy difference between the various isomer configurations of the clusters show that SCME/f gives good agreement with results of electronic structure calculations and represents a significant improvement over the previously presented rigid SCME potential function. Analysis of the vibrational frequencies of the clusters and structural properties of ice Ih crystal show the importance of accurately describing the variation of the quadrupole moment with molecular structures.

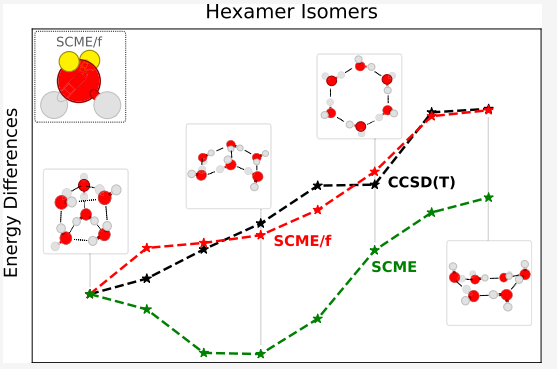

1. INTRODUCTION

The most commonly used potential energy functions for describing water molecules and their interaction are based on simple pairwise additive functions with fixed point charges,[1−4] such as the well-known TIPnP and SPC force fields. Extensions of these potential functions to describe flexible molecules have been developed, such as aSPC/Fw[5] and q-TIP4P/F,[6] and they offer, for example, the possibility to include the effect of zero-point energy (ZPE). The point charge potential functions are typically parameterized in such a way as to reproduce a few thermally averaged properties of liquid water. The properties of water molecules are, however, strongly environment dependent, as illustrated by the molecular dipole moment, which is 1.8 D in the gas phase and 3.1 D in ice Ih.[7] This large environment dependence needs to be modeled accurately in order to develop a transferable potential function applicable, for example, to small clusters and crystal structures as well as liquid water.

Such environment dependence is best described using well-established physical laws since empirical fitting to some limited set of data is likely not going to work well when the potential function is applied to configurations that are significantly different from the ones used in the fitting process. A systematic multipole expansion up to and including the hexadecapole, with dipole and quadrupole polarizability, has been shown to reproduce well the electrostatics in water clusters and ice.[8] A potential function based on this approach has been presented for rigid molecules and is referred to as the single-center multipole expansion (SCME) potential function.[9,10] In the present work, this approach is extended to flexible molecules.

By expanding the electrostatics around a single center on each molecule, the introduction of point charges and resulting charge−charge and charge−multipole interactions is avoided, and the correct long-range distance dependence of the Coulombic potential due to the neutral H_2O molecule is built in naturally. The leading term, the dipole potential, decays as $1/R^3$, and combined with the polarization response of the molecules, this makes it possible to use a long-range cutoff for the electrostatic interaction between molecules in typical condensed matter simulations.[7] Note however that the use of a single center for each molecule is only sufficient for small enough molecules.

Hybrid simulation schemes, where part of the system is simulated using a potential function while another part is described using electronic structure calculations, the so-called quantum mechanics/molecular mechanics (QM/MM) simu-

Received: June 8, 2022
Published: November 17, 2022

lations have been used in important simulation studies in various fields such has biochemistry,[11−15] medicine,[16] photochemistry,[17] solvation dynamics,[18−21] nanostructures,[22] and materials science.[23] In most cases, such simulations make use of fixed point charge models,[24−27] thereby neglecting the mutual polarization of the charges in the MM subsystem by the QM subsystem—an effect that was, however, included in the inceptive work initiating the QM/MM approach.[28] The use of fixed point charge models to represent water molecules in the MM region results in errors that limit the applicability of the QM/MM method.

Several H_2O potential functions that include some level of polarizability at the atomic or molecular sites exist.[29−31] These functions include the Thole-type multipole models such as the TTMn series[32−35] and HBB2-pol.[36,37] An alternative philosophy to the present single-site potential is the fully distributed point multipole models such as ASP-W4,[38] DPP2,[39] and derived intermolecular force field (DIFF)[40] potential functions. These potentials are based on a careful decomposition of the monomer properties and intermolecular interaction terms derived from the water dimer and include atomic site electrostatic, dispersion, repulsion, charge penetration, and charge delocalization terms. DIFF[40] includes atomic polarizabilities up to third rank and describes well the total and relative interaction energy of small and large water clusters, while being fitted only to water dimer properties. Distributed multipole approaches, however, lead to the introduction of point charges and thereby long-range Coulombic interactions which are problematic for condensed phase simulations.

The MB-pol[41−43] potential function has arguably reached the highest precision as it includes an explicit treatment of two-body and three-body interactions through an intricate permutationally invariant polynomial fit to large data bases constructed with high-level quantum chemistry calculations. However, inclusion of such explicit many body terms makes the interfacing with a QM region more challenging. Instead, simpler polarizable MM potential functions based on pair-wise potentials to describe the short-range interactions are used in the so-called polarizable embedding QM/MM (PE-QM/MM) approach.[26,44−74] The PE-QM/MM approach can be used to study the effects of solvation and solvent response to excitations and charge transfer in solvated species. However, such simulations have typically included only the molecular dipole−dipole response and make use of atomic point charges.

Here, we describe an extension of the SCME[9,10] potential function, which has recently been integrated in a PE-QM/MM scheme.[75,76] While the effort of the QM calculation often dominates the computational cost in non-polarizable QM/MM simulations, this is not necessarily the case in PE-QM/MM calculations where the self-consistent solution of the polarizable MM and QM are coupled.[75] Hence, it is desirable to keep the number of electrostatically coupled MM sites to a minimum. Our potential function includes the minimum number of sites per MM molecule and is therefore efficient for QM/MM calculations. The extended potential function, SCME/f, includes flexibility of the internal geometry of the water molecules while still maintaining the single-center description of the electrostatic interaction in terms of molecular moment tensors. The SCME/f model includes variable dipole and quadrupole moment tensors that depend on the geometry of the H_2O molecule. The dipole is described by the well-established Partridge−Schwenke (PS) model,[77] but a new, geometrical model based on four sites is presented here for the quadrupole moment. It reproduces results of high-level multireference electronic structure calculations of the quadrupole moment to within 1.6% RMS over a broad range in its magnitude. This model for the quadrupole moment is found to provide better description than the so-called M-site models that have been used previously.[2,3,32−37,41−43,78−80]

There are five adjustable parameters in the description of the intermolecular interaction. They include parameters relating to the pair-wise repulsive interaction, a damping parameter in the dispersion interaction, and a screening parameter for the electrostatic interaction tensors. These parameters are optimized in such a way that the SCME/f reproduces the binding energy and intermolecular distance of the dimer, the interaction energy of the lowest energy conformation of water clusters $(H_2O)_n$ with n ranging from 3 to 6, calculated at the level of RI-MP2 with CCSD(T) corrections[81] and full CCSD(T) at the complete basis set limit[82] as well as measured properties of crystalline ice Ih taking into account the ZPE. The resulting parametrization of the model reproduces nicely trends in the relative energy of the conformers of the hexamer obtained from high-level quantum chemistry calculations. Some discrepancies, however, exist in the series of pentamer isomers. An analysis of the frequency of vibrational modes of the various clusters and the structure of ice Ih crystal highlights the importance of an accurate model for the molecular quadrupole moment.

The article is organized as follows: the SCME/f potential function is described in Section 2. The dipole and quadrupole surfaces are presented in Section 3, and the calculation of atomic forces is described in Section 4. The fitting of the five adjustable parameters is described in Section 5, and comparison with ab initio data on the cluster conformer energy and vibrational frequencies of small clusters is described in Section 6. Discussion and conclusions are described in Section 7.

2. FLEXIBLE SCME MODEL

Figure 1 shows the principal vectors which define both the position of the expansion center and the local-to-global reference frame rotation matrix for the flexible water molecule. The local frame origin is placed at the center of mass (COM). In SCME/f, each water molecule is ascribed a molecular dipole and quadrupole moments in terms of variable partial charges based on the internal geometry, $\mu_\alpha^i(\{\boldsymbol{r}^{ia}\})$ and $\theta_{\alpha\beta}^i(\{\boldsymbol{r}^{ia}\})$, respectively, where $\{\boldsymbol{r}^{ia}\} = \{\boldsymbol{r}^{i\mathrm{O}}, \boldsymbol{r}^{i\mathrm{H}_1}, \boldsymbol{r}^{i\mathrm{H}_2}\}$, and is the set of position vectors for atoms a in molecule i in the global reference frame. The details of the dipole moment surface (DMS) and quadrupole moment surface (QMS) are described in Section 3. The index i is used to denote both the specific water molecule and the corresponding COM site. Furthermore, each water molecule is ascribed, in the local reference frame, a fixed octupole, $\Omega_{\alpha\beta\gamma}^{i'}$, and hexadecapole, $\Phi_{\alpha\beta\gamma\delta}^{i'}$, moment tensors, as well as polarizability tensors including dipole−dipole, $\alpha_{\alpha\beta}^{i'}$, dipole-quadrupole, $A_{\alpha\beta\gamma}^{i'}$, and quadrupole−quadrupole, $C_{\alpha\beta\gamma\delta}^{i'}$, induction terms.

Lipparini et al.[83] describe commonly used local reference frames and associated rotation matrices. The derivation here follows closely their work, with some obvious sign changes. The expansion center is placed at the COM

https://doi.org/10.1021/acs.jctc.2c00598
J. Chem. Theory Comput. 2022, 18, 7528−7543

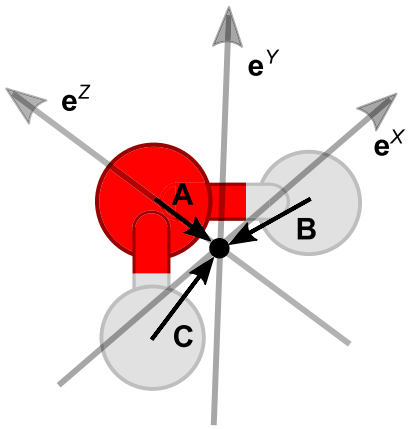

Figure 1. Definition of the principal vectors and local reference frame for the water molecule used in the SCME/f model. The black circle denotes the expansion center, chosen here to be at the COM. Black arrows show the three principal vectors ***A***, ***B***, and ***C*** pointing *from* the oxygen and the hydrogen atoms *to* the expansion center. The gray opaque arrows show the local reference frame basis vectors $\{\boldsymbol{e}^X, \boldsymbol{e}^Y, \boldsymbol{e}^Z\}$. The principal vectors ***B*** and ***C*** define a local-to-global reference frame rotation matrix. Due to the symmetry, specific indexing of the atoms is omitted, and positions and scales are exaggerated for clarity.

$$\boldsymbol{r}^i = \sum_a^{n_i} \boldsymbol{r}^{ia} \frac{M^a}{M^i} \tag{1}$$

where n_i denotes the atomic sites $\{O,H_1,H_2\}$ of molecule i, and M^a and M^i are the mass of the atom and molecule, respectively. The principal vectors used to define the rotation are

$$\boldsymbol{B}^i = \boldsymbol{r}^i - \boldsymbol{r}^{iH_1}, \qquad \boldsymbol{C}^i = \boldsymbol{r}^i - \boldsymbol{r}^{iH_2} \tag{2}$$

where in general, that is for a flexible H_2O molecule, $B^i \neq C^i$. Unit basis vectors are in terms of the principal vectors given by

$$\begin{aligned} \boldsymbol{e}^{iZ} &= \frac{B^i\boldsymbol{C}^i + C^i\boldsymbol{B}^i}{|B^i\boldsymbol{C}^i + C^i\boldsymbol{B}^i|} \\ \boldsymbol{e}^{iX} &= \frac{\boldsymbol{B}^i - (\boldsymbol{B}^i\cdot\boldsymbol{e}^{iZ})\boldsymbol{e}^{iZ}}{|\boldsymbol{B}^i - (\boldsymbol{B}^i\cdot\boldsymbol{e}^{iZ})\boldsymbol{e}^{iZ}|} \\ \boldsymbol{e}^{iY} &= \boldsymbol{e}^{iZ} \times \boldsymbol{e}^{iX} \end{aligned} \tag{3}$$

where $\boldsymbol{e}^{iZ}$ is, as defined above, the bisector between the two oxygen−hydrogen bonds. In terms of the unit basis vectors, a unitary local-to-global reference frame rotation matrix is

$$\boldsymbol{R}^i = \begin{bmatrix} e_x^{iX} & e_y^{iX} & e_z^{iX} \\ e_x^{iY} & e_y^{iY} & e_z^{iY} \\ e_x^{iZ} & e_y^{iZ} & e_z^{iZ} \end{bmatrix} \tag{4}$$

Given the rotation matrix for each molecule, the fixed moment and polarizability matrices are rotated into the global reference frame for each COM site i[a]

$$M^i_{\alpha\cdots\delta} = R^i_{\eta\alpha}\cdots R^i_{\sigma\delta} M^{i'}_{\eta\cdots\sigma} \tag{5}$$

where $M^i_{\alpha\cdots\delta}$ is a generalized tensor of order t, requiring t rotation operations (e.g., $\alpha^i_{\alpha\beta} = R^i_{\eta\alpha}R^i_{\tau\beta}\alpha^{i'}_{\eta\tau}$). With the definitions above, atomic forces are derived (see the Supporting Information) from the contribution of the fixed moments and polarizabilities to the electrostatic interactions involving the single expansion center on each molecule.

General formulation, and notation, of the perturbative expansion of the electrostatic intermolecular interaction—resulting in the multipole moment model—can be found elsewhere.[84] Here, we only present the main expressions which are used to arrive at a self-consistent solution to polarized molecular moments at sites i in response to the external field due to all other neighboring molecules $j(\neq i)$.

Given the external field, V^i_α (gradient of the scalar electrostatic potential), and the external field gradient, $V^i_{\alpha\beta}$, at the COM of i, the molecules are polarized, resulting in induced dipole and quadrupole moments

$$\Delta\mu^i_\alpha = -\alpha^i_{\alpha\beta}V^i_\beta - \frac{1}{3}A^i_{\alpha\beta\gamma}V^i_{\beta\gamma} \tag{6}$$

$$\Delta\theta^i_{\alpha\beta} = -A^i_{\gamma\alpha\beta}V^i_\gamma - C^i_{\gamma\delta\alpha\beta}V^i_{\gamma\delta} \tag{7}$$

where the external field is given by

$$V^i_\alpha = \sum_{j\neq i}^{n} V^{ij}_\alpha \tag{8}$$

and the contribution to the external field at site i due to site j is given by

$$\begin{aligned} V^{ij}_\alpha = &-T^{ij}_{\alpha\beta}(\mu^j_\beta(\{\boldsymbol{r}^{jb}\}) + \Delta\mu^j_\beta) \\ &+ \frac{1}{3}T^{ij}_{\alpha\beta\gamma}(\theta^j_{\beta\gamma}(\{\boldsymbol{r}^{jb}\}) + \Delta\theta^j_{\beta\gamma}) - \frac{1}{15}T^{ij}_{\alpha\beta\gamma\delta}\Omega^j_{\beta\gamma\delta} \\ &+ \frac{1}{105}T^{ij}_{\alpha\beta\gamma\delta\epsilon}\Phi^j_{\beta\gamma\delta\epsilon} \end{aligned} \tag{9}$$

The field gradient—and higher order gradients—are given by the subsequent use of the gradient operator, $\nabla_\beta V^i_\alpha = V^i_{\alpha\beta}$, $\nabla_\gamma V^i_{\alpha\beta} = V^i_{\alpha\beta\gamma}$.

At the start, the external field and field gradient due to the intrinsic moments are evaluated at each site. This results in an induced dipole and quadrupole moment, which in turn results in a change in the external field and field gradient. A self-consistent solution to the non-linear relation between eqs 6−9 is achieved with an iterative procedure and a suitable convergence threshold of the induced moments to achieve energy-force consistency (see the Supporting Information).

As the point moments come close, the multipole moment expansion breaks down—resulting in the so-called polarization catastrophe.[85] In order to avoid this, screened interaction tensors are introduced,[85−90] which effectively smear out the point moments. To the zeroth order, the Coulombic interaction tensors in eq 9 are defined as

$$T^{ij} = \frac{1}{r}\lambda_0(r) \tag{10}$$

where $r = |\boldsymbol{r}^j - \boldsymbol{r}^i|$, and $\lambda_0(r)$ is a short-range electrostatic interaction screening function. The gradient operators act to increase the order of the screened interaction tensors, for example

$$\nabla_\alpha T^{ij} = T^{ij}_\alpha \equiv -\frac{r_\alpha}{r^3}\lambda_1(r) \tag{11}$$

$$\nabla_\beta T^{ij}_\alpha = T^{ij}_{\alpha\beta} \equiv 3\frac{r_\alpha r_\beta}{r^5}\lambda_2(r) - \frac{\delta_{\alpha\beta}}{r^3}\lambda_1(r) \tag{12}$$

where $r_\alpha = (\boldsymbol{r}^j - \boldsymbol{r}^i)_\alpha$.

https://doi.org/10.1021/acs.jctc.2c00598
J. Chem. Theory Comput. 2022, 18, 7528−7543

Most commonly used interaction tensor screening functions in the context of polarizable force fields are based on the exponential decay of the point charges, resulting in the Thole-type damped tensors.[85] Here, we make use of screening functions derived from considering the overlap and resulting Coulombic electrostatic screening of Gaussian charge densities and multipoles.[89] In the equations above, they are

$$\lambda_0(r) = \mathrm{erf}(S) \tag{13}$$

$$\lambda_1(r) = \mathrm{erf}(S) - \frac{2}{\sqrt{\pi}} S e^{-S^2} \tag{14}$$

$$\lambda_2(r) = \mathrm{erf}(S) - \frac{2}{\sqrt{\pi}}\left(S + \frac{2}{3}S^3\right)e^{-S^2} \tag{15}$$

where S is the screened distance, $S = r/g$, and g is the screening length—describing the spatial extent of the Gaussian functions.

In the SCME/f model, the total energy is a function of the external field, V^i_α, at each molecular COM site i and is given by

$$E_{\mathrm{tot}}[\{V^i_\alpha\}] = E_{\mathrm{elst}}[\{V^i_\alpha\}] + E_{\mathrm{non-elst}} + E_{\mathrm{mon}} \tag{16}$$

where the terms on the right-hand side are, $E_{\mathrm{elst}}[\{V^i_\alpha\}]$, the total electrostatic energy functional, the non-electrostatic terms, $E_{\mathrm{non\text{-}elst}}$, which includes a pair-wise repulsive and a dispersion potential, and E_{mon}, which is a sum of the internal energies described by the Partridge-Schwenke potential energy surface (PS-PES) of the water monomer.[77]

More explicitly, the first term on the right-hand side of eq 16 can be further separated into three terms describing the inter- and intramolecular contributions to the total electrostatic energy of the system, namely

$$E_{\mathrm{elst}}[\{V^i_\alpha\}] = E_{\mathrm{in}}[\{V^i_\alpha\}] + E_{\mathrm{pol}}[\{V^i_\alpha\}] + E_{\mathrm{self}}[\{V^i_\alpha\}] \tag{17}$$

where $E_{\mathrm{in}}[\{V^i_\alpha\}]$ is the electrostatic interaction between the intrinsic molecular moments and $E_{\mathrm{pol}}[\{V^i_\alpha\}]$ is the field-induced polarization energy. At self-consistency, these terms combine to give

$$\begin{aligned} E_{\mathrm{in+pol}}[\{V^i_\alpha\}] = \frac{1}{2}\sum_i^n \Bigg(& (\mu^i_\alpha(\{\boldsymbol{r}^{ia}\}) + \Delta\mu^i_\alpha)V^i_\alpha \\ & + \frac{1}{3}(\theta^i_{\alpha\beta}(\{\boldsymbol{r}^{ia}\}) + \Delta\theta^i_{\alpha\beta})V^i_{\alpha\beta} \\ & + \frac{1}{15}\Omega^i_{\alpha\beta\gamma}V^i_{\alpha\beta\gamma} + \frac{1}{105}\Phi^i_{\alpha\beta\gamma\delta}V^i_{\alpha\beta\gamma\delta}\Bigg) \end{aligned} \tag{18}$$

E_{self} is the onsite self-energy, given by

$$E_{\mathrm{self}}[\{V^i_\alpha\}] = -\frac{1}{2}\sum_i^n \left(\Delta\mu^i_\alpha V^i_\alpha + \frac{1}{3}\Delta\theta^i_{\alpha\beta}V^i_{\alpha\beta}\right) \tag{19}$$

and accounts for the change in internal energy required to polarize the molecules.

The non-electrostatic term is composed of two intermolecular pair-wise potentials centered on the oxygen atom

$$E_{\mathrm{non-elst}} = E_{\mathrm{rep}} + E_{\mathrm{disp}} \tag{20}$$

describing repulsion, E_{rep}, and dispersion E_{disp}. In the following expressions, for the potentials the distance r refers to the oxygen−oxygen distance between pair i and j, or $r = |\boldsymbol{r}^{iO} - r^{iO}|$.

We make use of the same dispersion coefficients as in the original SCME model.[91] The dispersion energy is

$$E_{\mathrm{disp}} = -\sum_i^n \sum_{j<i}^n \left(\frac{C_6}{r^6}t_6(r) + \frac{C_8}{r^8}t_8(r) + \frac{C_{10}}{r^{10}}t_{10}(r)\right) \tag{21}$$

with isotropic coefficients up to tenth order from Wormer and Hettema.[92] At the short range, the interaction is smoothly switched off with a Tang−Toennies damping function[93]

$$t_m(r) = 1 - e^{-\tau_d r}\sum_{k=0}^m \frac{(\tau_d r)^k}{k!} \tag{22}$$

where the parameter τ_d represents the inverse decay length of the charge density.

In the rigid SCME[91] model, a modified Born−Mayer potential is used, which includes a term which scales the magnitude of the repulsion depending on the local environment around the repulsion center—a molecular density-dependent term. With the introduction of the Gaussian-type interaction tensor screening function, we find the molecular density dependence unnecessary and revert back to the basic Born−Mayer-type potential. The pair-wise repulsion is

$$E_{\mathrm{rep}} = \sum_i^n \sum_{j<i}^n A_{\mathrm{rep}} r^{-k} e^{-hr} \tag{23}$$

The parameters of the non-electrostatic terms, τ_d, A_{rep}, k, and h, are optimized to work with the new SCME/f model. The optimization also includes the screening length parameter g of eq 15. The fitting is described in Section 5.

3. DIPOLE AND QUADRUPOLE MOMENT SURFACES

The internal energy as described by the PS-PES includes analytical atomic force components,[77] as well as an accurate mapping of the DMS for an isolated water molecular as a function of the internal geometry. The DMS is given by

$$\mu^i_\alpha(\boldsymbol{r}^{iO}, \boldsymbol{r}^{iH_1}, \boldsymbol{r}^{iH_2}) = q^{iH_1}r^{iH_1}_\alpha + q^{iH_2}r^{iH_2}_\alpha + q^{iO}r^{iO}_\alpha \tag{24}$$

where $q^{iO} = -(q^{iH_1} + q^{iH_2})$ and the partial charges of the two hydrogens are in turn a function of the internal geometry, fitted to recreate the calculated DMS. For example $q^{iH_1} = q^{iH_1}(r^{OH_1}, r^{OH_2}, \cos(\theta_{\mathrm{HOH}}))$, where r^{OH_1} and r^{OH_2} are the internal bond lengths between the oxygen and the two hydrogens, and θ_{HOH} is the HOH angle. We make use of this mapping and leave it unchanged.

The DMS partial charges are not suitable to describe a QMS without modification. Instead, the charge site associated with the oxygen is split up into two components and placed within a plane perpendicular to the symmetry plane of the hydrogens and oxygens. The sites are denoted L_1 and L_2, where the site positions are directly related to the length of the hydrogen bond lengths indexed H_1 and H_2, and the HOH angle, see Figure 2. The QMS is written as

$$\begin{aligned} & \theta^i_{\alpha\beta}(\boldsymbol{r}^{iO}, \boldsymbol{r}^{iH_1}, \boldsymbol{r}^{iH_2}) \\ & = \sum_a^{n_i'} \frac{3}{2}\left\{q^{ia}\left((\boldsymbol{r}^{ia} - \boldsymbol{r}^i)_\alpha(\boldsymbol{r}^{ia} - \boldsymbol{r}^i)_\beta - \frac{\delta_{\alpha\beta}}{3}\|\boldsymbol{r}^{ia} - \boldsymbol{r}^i\|\right)\right\} \end{aligned} \tag{25}$$

where n_i' denotes the sites $\{H_1', H_2', L_1, L_2\}$ associated with molecule i. The apostrophe on the hydrogen is used to discern their role in the QMS from their role in the DMS since the charges $q^{iH_l'}$ are different from the DMS charges and are

https://doi.org/10.1021/acs.jctc.2c00598
J. Chem. Theory Comput. 2022, 18, 7528−7543

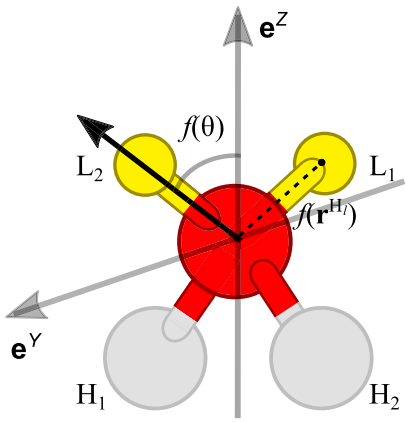

Figure 2. L-site placement (yellow) in the water monomer structure. The relationship of the angle to the unit basis vectors which describe the local reference frame is shown, eqs 32, 29, and 30. For example, operating with the rotation vector corresponding to hydrogen indexed 1 on e_α^{iZ} results in $(\cos(f(\theta))e_\alpha^{iZ} - \sin(f(\theta))e_\alpha^{iY})$. Due to the symmetry, specific indexing of the atoms is completely interchangeable, and either pair of H and L in the figure above can serve as pair 1 or 2. The distance from the oxygen to a L-site, controlled with $f(\boldsymbol{r}^{H_l})$ is a second-order polynomial function depending on the position of one of the hydrogens (while the position of the other L-site depends on the other hydrogen), eq 31. Positions and scales are exaggerated for clarity.

$$q^{iH_l'} = \mathrm{A}q^{iH_l} + \mathrm{B}q_{\mathrm{eq}}^{H} \tag{26}$$

and for the L-sites, they are

$$q^{iL_l} = \mathrm{C}q^{iH_l} + \mathrm{D}q_{\mathrm{eq}}^{H} \tag{27}$$

where q_{eq}^{H} is the DMS charge of the hydrogen in the equilibrium monomer configuration.

The position of the L_1 and L_2 charge sites is related to the atomic positions of each water molecule through a rotation operator times a scaling factor which controls the length of the rotated vector. A translation operator translates the vector to the COM position of molecular site i for completeness. Explicitly, this operation is

$$r_\alpha^{iL_l} = R_{\eta\alpha}^{iL_l} e_\eta^{iZ} f(\boldsymbol{r}^{H_l}) + r_\alpha^{i} \tag{28}$$

We make use of the unit basis vectors previously used to define the local-to-global rotation matrices in eqs 1−3. The rotation matrices for the L_1 and L_2 sites are

$$\boldsymbol{R}^{iL_1} = (\cos(f(\theta))\boldsymbol{I} - \sin(f(\theta))[\boldsymbol{e}^{iX}]_\times) \tag{29}$$

$$\boldsymbol{R}^{iL_2} = (\cos(f(\theta))\boldsymbol{I} + \sin(f(\theta))[\boldsymbol{e}^{iX}]_\times) \tag{30}$$

and is a simplification of the general Rodrigues' rotation operator[94] in terms of the local orthonormal basis vectors (as shown in Figure 1).

In order to allow for flexibility of the L-sites and correlate their positions to the change in the positions of the hydrogens, both the angle factor and length scale factor are defined in terms of the OH bond lengths and HOH angle through

$$f(\boldsymbol{r}^{H_l}) = a + b(|\boldsymbol{r}^{iO} - \boldsymbol{r}^{iH_l}| - r_{\mathrm{eq}}) + c(|\boldsymbol{r}^{iO} - \boldsymbol{r}^{iH_l}| - r_{\mathrm{eq}})^2 \tag{31}$$

$$f(\theta) = d + e(\theta - \theta_{\mathrm{eq}}) \tag{32}$$

where r_{eq} and θ_{eq} are the equilibrium hydrogen to oxygen bond length and HOH angle of the isolated PS-PES water molecule, respectively, see Figure 2. We find that a second-order polynomial in terms of the change in the bond length, and a linear term for the change in bond angles, is adequate to capture the QMS with good accuracy. The charge scaling parameters A, B, C, and D, and the geometric parameters a, b, c, d, and e are fitted parameters, described below.

3.1. Ab Initio QMS Calculations and Fit. The dipole and quadrupole moment is mapped using ab initio quantum chemistry software ORCA.[95,96] An iterative-configuration expansion configuration interaction (ICE-CI) method is used, with the aug-cc-pvqz basis set, and the energy convergence threshold is set to 10^{-8} Eh. Eight correlated electrons are included, and the active orbitals were chosen by including MP2 orbitals of natural orbital occupation numbers ranging between 1.99999 and 0.00001. The ICE-CI method is related to the CIPSI technique.[97] Note that this level of theory is necessary to accurately determine the dipole and quadrupole moment using their well-defined charge density-based operators, instead of resorting to energy-based schemes to estimate these quantities. For example, we find that coupled-cluster at the CCSD(T)/aug-cc-pvqz level of theory and orbital optimized coupled-cluster theory OOCCSD(T)/aug-cc-pvdz, did not provide a satisfactory agreement with the DMS of the PS-PES, when using the dipole moment operator $\mu_\alpha = \int \rho(\boldsymbol{r}) r_\alpha \mathrm{d}\boldsymbol{r}$. See the Supporting Information for more details.

Starting from the ground-state geometry in the local-frame, as shown in Figure 1, the internal bond lengths and HOH angle are systematically changed and range from 0.7 to 1.3 and 60 to 175°, respectively. These intervals broadly represent the variation in the bond lengths and the angle of the water molecule in the liquid phase under ambient conditions. Figure 3 shows a comparison between the internal energy change of each configuration, as calculated by the ICE-CI method compared to the PS-PES. The agreement is excellent and

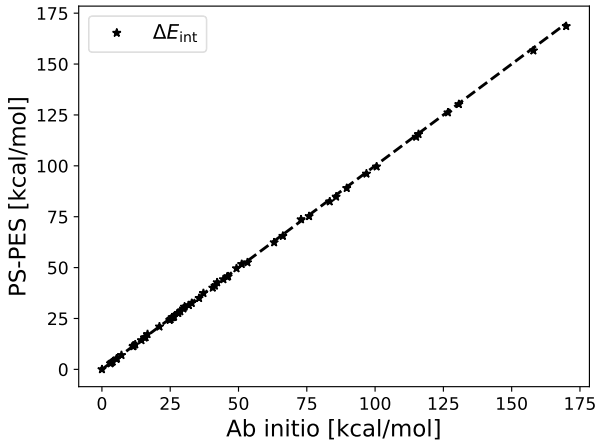

Figure 3. Relative internal energy difference between the different monomer configurations used in the QMS fit, compared between the ab initio results and the PS-PES. The good agreement between the two methods implies that the use of the ICE-CI data to fit the QMS justifies the use of the original PS−PES to represent internal energy changes and resulting atomic forces as both potential energy surfaces are close with RMSD of ∼0.51 kcal/mol, within chemical accuracy. An analysis of the deviation is presented in the Supporting Information.

https://doi.org/10.1021/acs.jctc.2c00598
J. Chem. Theory Comput. 2022, 18, 7528−7543

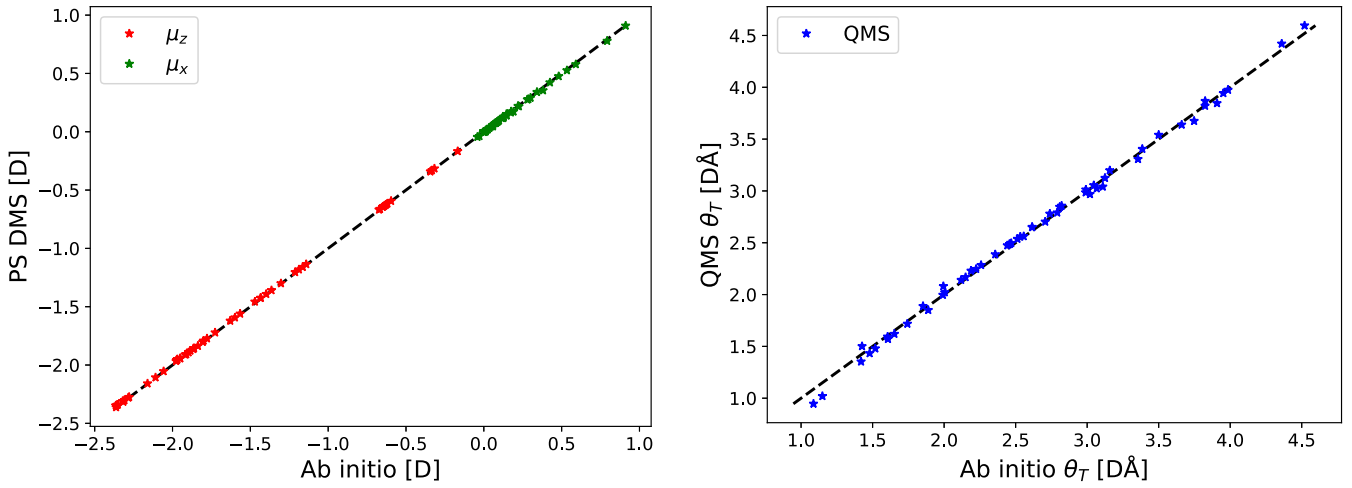

Figure 4. Left: comparison of the dipole z- and x-components, μ_z and μ_x, respectively, as predicted by the DMS, eq 24 and compared to the ICE-CI μ_z and μ_x. Note that due to a choice of the local reference frame, the μ_y component is always numerically zero. The DMS of the PS-PES and ICE-CI are in an excellent agreement, with a RMSD of 0.004 D and within 0.5% on average. Right: comparison of the θ_T component mapped by the QMS, eq 25, with the ab initio ICE-CI data. The geometric QMS model of this work, which is fitted to best reproduce the ab initio results, captures the results to a good degree with low scatter, a mean absolute error of 0.04 DÅ, and an average RMS difference of around 1.6% (see the Supporting Information for RMSD analysis).

justifies the use of the ab initio data to fit the QMS while retaining the original PS-PES energy mapping to describe the internal energy change and resulting atomic forces in our model. Figure 4, left, presents a comparison between the ICE-CI DMS and the PS-PES DMS, again in an excellent agreement.

The QMS model parameters associated with the charges in eqs 26 and 27, A, B, C and D, as well as the geometric parameters of eqs 31 and 32, a, b, c, d and e, are fitted to best reproduce the principal quadrupole moment component. Considering the water molecule in the ground-state configuration, the symmetric quadrupole moment tensor can be written as

$$\theta = \begin{bmatrix} \theta_T - \Delta & 0 & 0 \\ 0 & -\theta_T - \Delta & 0 \\ 0 & 0 & 2\Delta \end{bmatrix} \tag{33}$$

where $\theta_T = (\theta_{xx} - \theta_{yy})/2$.

The values of the QMS parameters are determined by carrying out a least-squares optimization, using a module freely available in the scientific computing package SciPy.[98] Table 1 presents the numerical values and units of the resulting best fit parameters, and Figure 4, right, shows the resulting fit of the θ_T components, compared between the QMS fit and ab initio ICE-CI values. The overall fit is in good agreement with the ab initio values over a broad range of θ_T values, with very low scatter. The largest deviation is found where θ_T is lowest, that is where the quadrupole moment interaction strength is the weakest.

Table 1. Numerical Values and Units of the Quadrupole Moment Surface Function, Eq 25

geometry		charges	
a [Å]	0.5149	A	0.9763
b	−1.1271	B	0.6418
c [Å^{-1}]	0.5146	C	0.7251
d [rad]	3.5908	D	−1.0603
e	−0.1081	q_{eq}^H	0.3310
r_{eq} [Å]	0.9578		
θ_{eq} [rad]	1.8240		

4. FORCES

With the various expressions given in the preceding section, analytical atomic force components can be obtained and are derived from the negative gradient of the total energy expression, eq 16, with respect to the position of atom a in molecule i, or

$$F_\alpha^{ia} = -\frac{dE_{tot}}{dr_\alpha^{ia}} = -\frac{\partial E_{elst}}{\partial r_\alpha^{ia}} - \frac{\partial E_{non-elst}}{\partial r_\alpha^{ia}} - \frac{\partial E_{mon}}{\partial r_\alpha^{ia}} \tag{34}$$

The first term on the right-hand side results in several contributing factors to the atomic forces due to the definition of the principal axes, choice of expansion center, and the DMS and QMS. The atomic forces resulting from the simple pairwise potentials describing the non-electrostatic terms are omitted for the sake of brevity, and the atomic forces due to the monomer energy expression—the PS-PES—are accounted for in their original work.[77]

The first term on the right-hand side of eq 34, the total intermolecular electrostatic interaction, can be further divided into four contributions

$$-\frac{\partial E_{elst}}{\partial r_\alpha^{ia}} = -\frac{\partial E_{elst}}{\partial \mu_\beta^j(\{\boldsymbol{r}^{jb}\})}\frac{\partial \mu_\beta^j(\{\boldsymbol{r}^{jb}\})}{\partial r_\alpha^{ia}} - \frac{\partial E_{elst}}{\partial \theta_{\beta\gamma}^j(\{\boldsymbol{r}^{jb}\})}\frac{\partial \theta_{\beta\gamma}^j(\{\boldsymbol{r}^{jb}\})}{\partial r_\alpha^{ia}} - \frac{\partial E_{elst}}{\partial V_{\beta\gamma\delta\epsilon\cdots\eta}^j}\frac{\partial V_{\beta\gamma\delta\epsilon\cdots\eta}^j}{\partial r_\alpha^{ia}} - \frac{\partial E_{elst}}{\partial R_{\eta\beta}^j}\frac{\partial R_{\eta\beta}^j}{\partial r_\alpha^{ia}} \tag{35}$$

https://doi.org/10.1021/acs.jctc.2c00598
J. Chem. Theory Comput. 2022, 18, 7528−7543

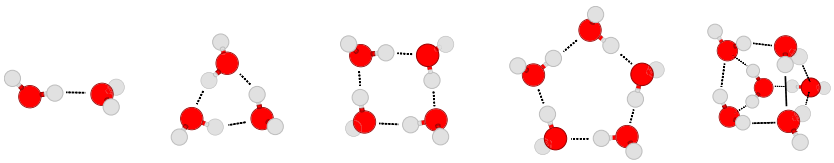

Figure 5. Lowest lying water cluster $(H_2O)_n$ isomers for $n = 2-6$ used in the fitting procedure for the model parameters. From left to right; dimer (Cs), trimer (UUD), quadromer (S4), pentamer (cyclic, CYC), and hexamer (prism, PRI).

which are, in order, the partial derivative of the DMS and QMS, partial derivative of the external field and gradients thereof, and partial derivatives of the local-to-global rotation matrices, as defined in eqs 1−4.

At self-consistency of the iterative process which minimizes the energy in terms of the polarized moments, the following conditions apply

$$\frac{\partial E_{\mathrm{elst}}}{\partial \Delta\mu_\alpha^i} = \frac{\partial E_{\mathrm{elst}}}{\partial \Delta\theta_{\alpha\beta}^i} = \frac{\partial E_{\mathrm{self}}}{\partial \Delta\mu_\alpha^i} = \frac{\partial E_{\mathrm{self}}}{\partial \Delta\theta_{\alpha\beta}^i} = 0$$

There are no explicit force contributions from the self-energy terms due to the onsite external field as the self-energy can be written solely in terms of the onsite induced moments (see the Supporting Information). This results in a non-trivial additional condition

$$\frac{\partial E_{\mathrm{self}}}{\partial V_{\beta\gamma\delta\epsilon\cdots\eta}^j} = 0 \tag{36}$$

Due to these conditions of the self-energy, a single force contribution arises and is due to the local-to-global transformation of the fixed polarizability tensors

$$-\frac{\partial E_{\mathrm{self}}}{\partial r_\alpha^{ia}} = -\frac{\partial E_{\mathrm{self}}}{\partial R_{\eta\beta}^j}\frac{\partial R_{\eta\beta}^j}{\partial r_\alpha^{ia}} \tag{37}$$

The total force contribution due to the intermolecular electrostatic interaction and intramolecular self-energy is then

$$\begin{aligned}
&-\left(\frac{\partial E_{\mathrm{in+pol}}}{\partial r_\alpha^{ia}} + \frac{\partial E_{\mathrm{self}}}{\partial r_\alpha^{ia}}\right) \\
&= -\frac{\partial E_{\mathrm{in+pol}}}{\partial \mu_\beta^j(\{\boldsymbol{r}^{jb}\})}\frac{\partial \mu_\beta^j(\{\boldsymbol{r}^{jb}\})}{\partial r_\alpha^{ia}} - \frac{\partial E_{\mathrm{in+pol}}}{\partial \theta_{\beta\gamma}^j(\{\boldsymbol{r}^{jb}\})}\frac{\partial \theta_{\beta\gamma}^j(\{\boldsymbol{r}^{jb}\})}{\partial r_\alpha^{ia}} \\
&\quad - \frac{\partial E_{\mathrm{in+pol}}}{\partial V_{\beta\gamma\delta\epsilon\cdots\eta}^j}\frac{\partial V_{\beta\gamma\delta\epsilon\cdots\eta}^j}{\partial r_\alpha^{ia}} - \left(\frac{\partial E_{\mathrm{in+pol}}}{\partial R_{\eta\beta}^i} + \frac{\partial E_{\mathrm{self}}}{\partial R_{\eta\beta}^i}\right)\frac{\partial R_{\eta\beta}^i}{\partial r_\alpha^{ia}}
\end{aligned} \tag{38}$$

The terms in the expression above are given explicitly in the Supporting Information. We note that in order to evaluate the first term on the right-hand side, explicit partial charge derivatives with respect to atomic positions of the DMS are required, which were not included in the original work on the PS-PES.[77] These are provided by Burnham and Xantheas, first used in the development of a flexible Thole-type multipole moment expansion potential.[32]

5. FLEXIBLE MODEL FIT

With the introduction of the DMS and QMS, the Gaussian-type interaction tensor screening functions, as well as the changes to the pair-wise repulsion function, all of the five model parameters which affect the intermolecular interactions g, τ_d, A_{ref}, k, and h are re-fitted. The fitting is performed with the same least-squares optimization module used for the QMS fit. We make use of the same numerical values for the fixed octupole and hexadecapole, as well as the dipole−dipole, dipole−quadrupole, and quadrupole−quadrupole polarizability as in the original SCME model.[10] The Fortran-based SCME/f code is freely available online[99] and includes an interface to the Python-based Atomic Simulation Environment[100,101] library.

The data set used for the fitting includes several points around the minimum of the dimer binding curve with the energy minimum and oxygen−oxygen distance corresponding to CCSD(T) calculations.[82] A single interaction energy for the lowest lying trimer, tetramer, pentamer, and hexamer is included. Figure 5 shows the geometry of the lowest-lying water clusters $(H_2O)_n$ in the range $n = 2-6$. The reference calculations which we make use of here include the complete basis set limit CCSD(T) energies of the low-lying water hexamer structures by Bates and Tschumper.[81] For the other cluster sizes—trimers, tetramers, and pentamers—complete basis set limit RI-MP2 calculations, with CCSD(T) corrections, are used.[82]

In addition to the clusters, we have also considered properties of hexagonal ice (ice Ih), which is the most common ice phase. There are no high-level first-principle calculations with sufficient accuracy to serve as reference values. Instead, we need to use the experimental data for lattice constants, unit cell volume, bulk modulus, and lattice energies, which generally include ZPE effects, and these effects are quite sizeable.[102−105] Consequently, we have performed phonon calculations with the SCME/f model for proton disordered units cells of ice Ih containing 96 water molecules using the Parlinski−Li−Kawazoe finite-displacement method,[106] as implemented in the PHONOPY package[107] using 3 × 3 × 3 supercells and a displacement of 0.01 Å. For a unit cell with fixed cell vectors, we have first performed a geometry relaxation employing the analytical SCME/f forces with a force threshold of 10^{-3} eV/Å. Then, using a 10 × 10 × 10 q-point sampling for the Brillouin zone integration, we obtain a numerically converged phonon density of states $g(\omega)$, the first moment of which provides the ZPE

$$E_{\mathrm{ZPE}} = \frac{\hbar}{2}\int_0^\infty \omega g(\omega)\mathrm{d}\omega \tag{39}$$

considering the dependence of the phonon frequencies on the unit cell volume $\omega = \omega(V)$ within the so-called quasi-harmonic approximation yields a ZPE-corrected energy−volume curve

$$E_{\mathrm{tot+ZPE}}(V) = E_{\mathrm{tot}}(V) + E_{\mathrm{ZPE}}(V) \tag{40}$$

where the energy zero is such that it describes infinitely separated (non-bound) individual water molecules. By fitting the Rose-Vinet equation of state,[108] we obtain the minimum $E_{\mathrm{lat}}^{\mathrm{ZPE}} = E_{\mathrm{tot+ZPE}}(V_0^{\mathrm{ZPE}})$ of that curve together with the ZPE-corrected bulk modulus B_0^{ZPE} (see the Supporting Information for more details), which can be compared against accurate

https://doi.org/10.1021/acs.jctc.2c00598
J. Chem. Theory Comput. 2022, 18, 7528−7543

experimental data.[102,109,110] In order to include this data in the fitting process, an initial $E_{tot+ZPE}(V)$ was calculated based on the SCME/f parameters first determined by fitting the data set derived from the water clusters. Then, $E_{tot}(V)$ was improved by further parameter adjustments such that the expected ZPE correction would bring it close to the experimental values. This trial and error scheme was found necessary since the phonon calculations are significantly more expensive than the calculation of the cluster properties. The end results based on a new set of phonon calculations are presented in Table 2

Table 2. Properties of Crystal Ice Ih Evaluated with SCME[9,10] and SCME/f, Compared to Experimental Values[a]

property	SCME	SCME/f	Exp.[b]
$\langle r_{OO}\rangle$ [Å]	2.742	2.751	2.751
a [Å]	4.470	4.478	4.497
b [Å]	7.747	7.777	7.789
c [Å]	7.287	7.331	7.321
V_0 [Å^3]	31.55	30.38	
V_0^{ZPE} [Å^3]		31.98	32.05
E_{lat} [eV]	−0.611	−0.645	−0.611
E_{lat}^{ZPE} [eV]		−0.489	−0.491
B_0 [GPa]	11.4	15.0	
B_0^{ZPE} [GPa]		12.2	10.9

[a] $\langle r_{OO}\rangle$ is the average oxygen−oxygen distance, and a, b, and c are the lattice parameters for a dipole-free orthorhombic cell (containing eight molecules). V_0^{ZPE} (V_0) is the optimized cell volume, and E_{lat}^{ZPE} (E_{lat}) and B_0^{ZPE} (B_0) are the lattice energy and bulk modulus with (and without) ZPE correction, all expressed per molecule. [b] Experimental values: average oxygen−oxygen distance is from,[119] lattice parameters from Röttger et al.[109] (and resulting V_0^{ZPE}), enthalpy of vaporization (E_{lat}^{ZPE}) and lattice energy (E_{lat}) from Whalley,[102] and bulk modulus from Hobbs.[110]

and show good agreement with the experimental target properties (the concomitant energy−volume curves are shown in the Supporting Information). Table 3 compiles the concomitant final optimized parameters of the SCME/f model.

Table 3. Intermolecular Interaction Model Parameters, Numerical Values, and Units

damping		repulsion	
τ_d [Å^{-1}]	7.5548	A_{rep} [eV]	8149.63
g [Å]	1.1045	k	0.5515
		h [Å^{-1}]	3.4695

Table 4 shows the resulting interaction energy and relative interaction energy versus the reference CCSD(T) calculations of the lowest lying isomers used in the fit. This includes a structural analysis comparing the relaxed SCME/f structure to the CCSD(T) reference structures, where the RMS deviation of nearest neighbor oxygen−oxygen distances, $\langle dr_{OO}\rangle$, intramolecular oxygen-hydrogen bond lengths of the donor hydrogens, $\langle dr_{OH}\rangle$, hydrogen bonding (H-bond) bond lengths, $\langle dr_{O\cdots H}\rangle$, and angles between oxygen−hydrogen−oxygen in H-bonds, $\langle d\angle OHO\rangle$, are presented. The overall RMSD of the atomic positions is also presented, $\langle dr^a\rangle$, and is evaluated with the Kabsch algorithm.[111] The interaction energies for the different cluster sizes are reproduced to a reasonable degree, with sub kcal/mol difference compared to the CCSD(T) results, except for the prism isomer of the hexamer where the interaction energy is underestimated by 1.18 kcal/mol.

The resulting relaxed structures are in an overall very good agreement with the reference structures, with small variations in the second decimal in terms of atomic distances. Similarly, the angles between OHO in H-bonds are in a good agreement with the reference. The largest deviation is found in the angle between the donor−acceptor in the dimer.

6. MODEL VALIDATION

For further validation of the new model, the interaction energies and relative energy differences of all higher lying isomers of the pentamers and hexamers are calculated, which are not included in the fitting data set, and compared to the relative energies from the quantum chemistry.[81,82] The trends are shown in Figure 6, and the trend predicted with the rigid SCME is shown for comparison. All structures are relaxed with a force tolerance of 10^{-4} eV/Å, and results are collected in Table 5, which also presents the RMS difference between the relaxed SCME/f structures and the quantum chemistry reference structures.

For the pentamers, Figure 6 top, most of the relative energy difference trend is captured with the exception of isomer FRA, whose relative stability is underestimated. Another key difference between SCME/f and the reference calculations is the series of CAA−CAB isomers, which have a cage-like structure. In particular, the cage structure of isomers CAA and CAB are not stable and rearrange to isomers, which are more akin to the fused ring structures of the FRA−FRC isomers. The resulting SCME/f structures of CAA and CAB are near identical, with an interaction energy difference of only 0.01 kcal/mol. Only the CAC isomer maintains its cage-like structure, but one of the H-bonds is not stable (between a

Table 4. Interaction Energy (kcal/mol) and Distances (Å) between Atoms in the Most Stable Configuration of Clusters $(H_2O)_n$ with n = 2,...,6[a]

$(H_2O)_n$	E_{int}	ΔE_{int}	$\langle dr_{OO}\rangle$	$\langle dr_{OH}\rangle$	$\langle dr_{O\cdots H}\rangle$	$\langle dr^a\rangle$	$\langle d\angle OHO\rangle$
2-Cs	−4.85	+0.18	0.011	0.000	0.017	0.017	5.923
3-UUD	−15.16	+0.54	0.035	0.010	0.037	0.037	2.489
4-S4	−27.51	−0.11	0.005	0.014	0.006	0.045	1.382
5-CYC	−36.72	−0.71	0.014	0.015	0.003	0.046	0.369
6-PRI	−47.10	−1.18	0.017	0.012	0.035	0.033	4.564

[a] E_{int} is the SCME/f calculated interaction energy of the clusters and ΔE_{int} (kcal/mol) the difference with respect to the CCSD(T) values. $\langle dr_{OO}\rangle$, $\langle dr_{OH}\rangle$, and $\langle dr_{O\cdots H}\rangle$ are the RMSD of the oxygen−oxygen neighbor distances, intramolecular oxygen−hydrogen bond lengths of the donor-hydrogen, and bonding oxygen··· hydrogen bond length distances, respectively, compared to the CCSD(T) obtained structures.[81,82] $\langle dr^a\rangle$ is the overall RMSD of the relaxed SCME/f structure evaluated using the Kabsch algorithm.[111] All bond-related differences are shown in units Å. $\langle d\angle OHO\rangle$ is the RMSD of the angle (in degrees) between the oxygen−hydrogen−oxygen in hydrogen bonds.

https://doi.org/10.1021/acs.jctc.2c00598
J. Chem. Theory Comput. 2022, 18, 7528−7543

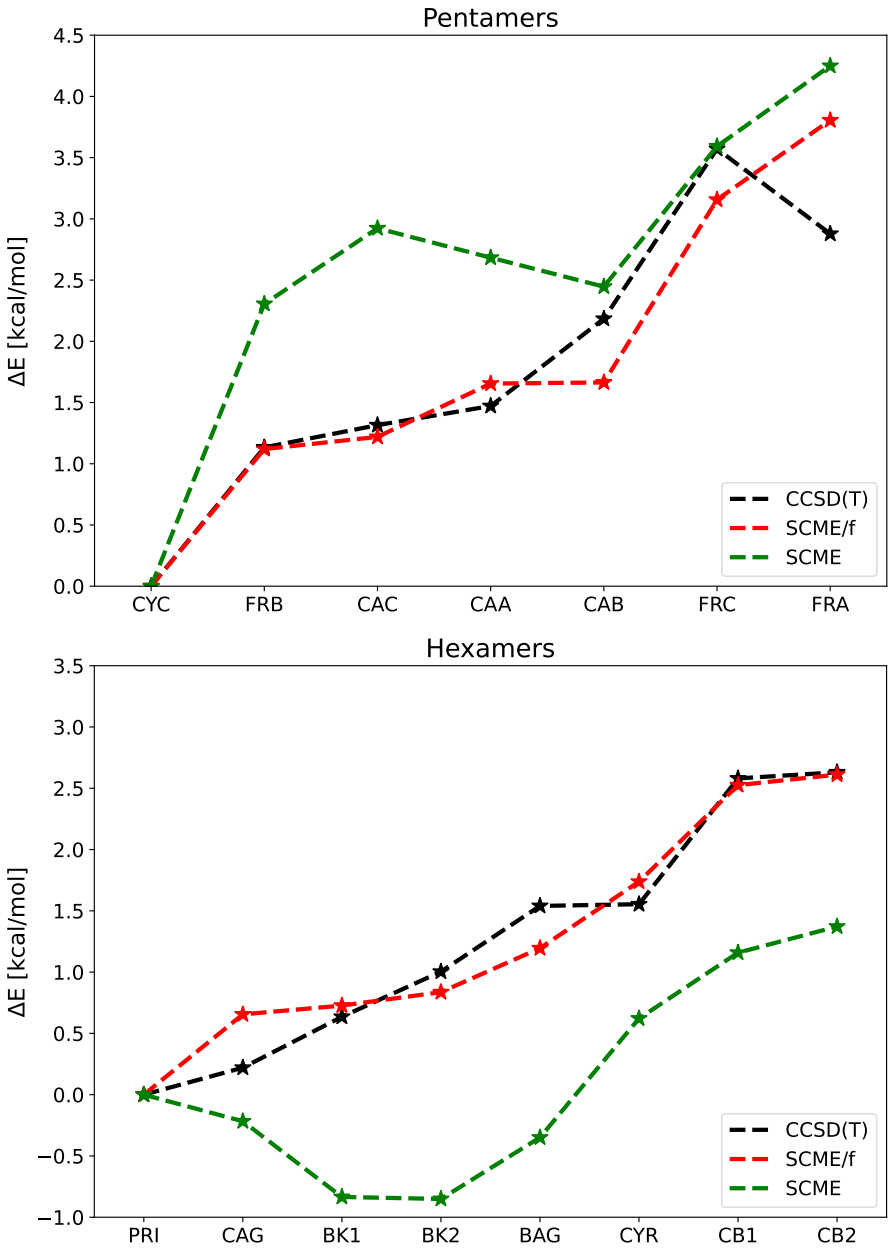

Figure 6. Relative energy difference for the lowest lying pentamers (top) and hexamer (bottom) water cluster isomers. The results for the rigid version of SCME[9,91] and SCME/f are compared. Relative energy differences from high-level quantum chemistry calculations are also shown; for the pentamers, these are RI-MP2 energies at the complete basis set limit with CCSD(T) corrections[82] [MP2/CBS + ΔCCSD(T)]; for the hexamers, these are CCSD(T) energies at the complete basis set limit [CCSD(T)/CBS].[81] The acronyms from left to right are the different isomers. Pentamers; cyclic (CYC), fused-ring-B (FRB), cage-C (CAC), cage-A (CAA), cage-B (CAB), fused-ring-C (FAC), and fused-ring-A (FRA); and the hexamers; prism (PRI), cage (CAG), book-1 (BK1), book-2 (BK2), bag (BAG), cyclic-ring (CYR), cyclic-boat-1 (CB1), and cyclic-boat-2 (CB2).

donor acceptor oxygen with distance greater than 3.0 Å), resulting in the rotation of one of the water monomers. Compared to the rigid SCME predecessor, this represents an improvement, in particular for the FRB, CAC, and CAA isomers, whose stability is greatly underestimated relative to the CYC isomer.

For the hexamers, Figure 6 bottom, the overall trend in the relative interaction energies is captured to a good degree compared to the CCSD(T) reference and is a substantial improvement over the rigid SCME model, which greatly underestimates the stability of the prism isomer relative to all other isomers. The bond lengths and angles of the hexamer isomers are all in very good agreement with the reference structures, with small differences in the second or third decimal in terms of the bond lengths, and the H-bonded OHO angles deviate by only 2−4°. Table 6 presents vibrational frequency analysis of the lowest lying isomers, including the cyclic ring isomer of the hexamer. The RMS deviations from near-CBS CCSD(T) calculations[112,113] are presented for the different classes of modes. These are intermolecular low-energy vibrational modes (10−1000 cm^{-1}), intramonomer bending modes (1600−1800 cm^{-1}), and H-bonded and non-bonded OH stretching modes (ca. 3200−3900 cm^{-1}). For comparison, the same analysis is performed for the SCME/f model but with

https://doi.org/10.1021/acs.jctc.2c00598
J. Chem. Theory Comput. 2022, 18, 7528−7543

Table 5. Energies and Relative Energy and Structural Properties of the Pentamer and Hexamer Isomers[a]

$(H_2O)_n$[b]	E_{int}	ΔE_{int}	$\langle dr_{OO}\rangle$	$\langle dr_{OH}\rangle$	$\langle dr_{O\cdots H}\rangle$	$\langle dr^a\rangle$	$\langle d\angle OHO\rangle$
5-FRB	−35.60	−0.72	0.026	0.012	0.041	0.036	4.008
5-CAC	−35.50	−0.81	0.053	0.012	0.089	0.136	8.548
5-CAA	−35.07	−0.53	0.060	0.012	0.053	0.254	9.281
5-CAB	−35.06	−1.23	0.065	0.011	0.080	0.237	6.107
5-FRC	−33.56	−1.12	0.025	0.013	0.026	0.043	1.859
5-FRA	−32.91	0.22	0.025	0.013	0.032	0.059	1.731
6-CAG	−46.44	−0.74	0.013	0.017	0.019	0.054	1.607
6-BK1	−46.37	−1.09	0.014	0.015	0.009	0.033	2.346
6-BK2	−46.26	−1.35	0.014	0.016	0.008	0.038	3.433
6-BAG	−45.90	−1.52	0.015	0.017	0.012	0.065	3.826
6-CYR	−45.36	−1.00	0.012	0.015	0.006	0.018	3.913
6-CB1	−44.57	−1.23	0.013	0.015	0.003	0.031	2.924
6-CB2	−44.49	−1.20	0.013	0.015	0.005	0.025	2.284

[a]See the caption of Table 4 for the definition of the table entries. [b]Pentamers; fused-ring-B (FRB), cage-C (CAC), cage-A (CAA), cage-B (CAB), fused-ring-C (FAC), and fused-ring-A (FRA); and the hexamers; cage (CAG), book-1 (BK1), book-2 (BK2), bag (BAG), cyclic-ring (CYR), cyclic-boat-1 (CB1), and cyclic-boat-2 (CB2).

Table 6. Relative Vibrational Properties of the Lowest Lying water Clusters, Including the Cyclic Ring Isomer of the Water Hexamer Cluster[a]

		quadrupole moment surface			fixed quadrupole moment		
$(H_2O)_n$		$\langle\Delta cm^{-1}\rangle$		max $\lvert\Delta cm^{-1}\rvert$	$\langle\Delta cm^{-1}\rangle$		max $\lvert\Delta cm^{-1}\rvert$
2-Cs	l	17.52		41.50	15.33		23.10
	b	6.71		9.10	9.18		12.70
	h	28.55		36.10	50.41		70.30
	t	**17.23**			**23.56**		
3-UUD	l	23.03		49.20	34.43		71.70
	b	7.75		12.20	18.41		23.90
	h	68.09		89.30	153.65		190.40
	t	**31.20**	(24.98)		**64.02**	(29.19)	
4-S4	l	20.87		44.40	29.43		58.10
	b	10.74		12.80	25.69		29.40
	h	155.58		200.20	266.11		334.10
	t	**59.19**	(21.06)		**100.25**	(26.49)	
5-CYC	l	18.47		35.20	35.08		65.30
	b	14.22		19.60	26.44		34.40
	h	179.34		229.60	282.41		358.10
	t	**66.02**	(20.13)		**105.22**	(31.38)	
6-CYR	l	21.10		44.30	35.16		75.40
	b	11.55		13.10	32.53		40.00
	h	185.38		239.30	280.06		356.30
	t	**67.75**	(23.24)		**103.48**	(32.56)	
6-PRI	l	21.70		87.60	27.74		56.20
	b	9.86		18.30	35.16		45.80
	h	208.58		408.60	313.99		571.80
	t	**75.79**	(24.60)		**113.85**	(36.40)	

[a]The entries for each system correspond from top to bottom, the low-frequency intermolecular vibrational modes (l, 10−1000 cm^{-1}), intramonomer bending (b, 1600−1800 cm^{-1}), and high-frequency stretching of H-bond OH and non-bonded OH bonds (h, 3200−3900 cm^{-1}). $\langle\Delta cm^{-1}\rangle$ is the RMSD between the frequencies in the low, medium, and high range, as predicted with SCME/f compared to near-CBS CCSD(T) reference calculations.[112,113] The last entry is RMSD for the total frequency range (**t**), where the value in the parenthesis excludes the overestimated H-bond OH stretches. max $\lvert\Delta cm^{-1}\rvert$ is the maximum absolute difference for each entry. The two columns on the right are for the SCME/f model potential with the quadrupole moment set to a fixed value corresponding to the ground-state water monomer configuration.

the quadrupole moment fixed and corresponding to the numerical value of the quadrupole moment for the ground-state monomer configuration.

With the inclusion of the QMS (left column Table 6), the low-energy vibrational modes and, in particular, the bending modes are in a good agreement with the reference calculations. The RMS deviation ranges from 18 to 23 and 7 to 14 cm^{-1} for the two classes of modes, respectively. The maximum difference in the bending modes does not exceed 20 cm^{-1} for any of the clusters analyzed. The red shift of the H-bonded OH stretches is, however, not captured by our model, resulting in an overestimation of these modes, which becomes systematically larger with cluster size. This is due to the underlying monomer potential energy surface, whose limit in terms of hydrogen dissociation is $OH^{\bullet} + H^{\bullet}$ whereas should be in the condensed phase $OH^{-} + H^{+}$. The model potential does

https://doi.org/10.1021/acs.jctc.2c00598
J. Chem. Theory Comput. 2022, 18, 7528−7543

not describe this important change and the resulting weakening of oxygen−hydrogen bonds in H-bonding OH. The high-frequency modes for the dimer are though in a reasonable agreement with the reference calculations.

A comparison to the same vibrational frequency analysis is performed with the quadrupole moment fixed (right column, Table 6). Fixing the quadrupole moment results in a drastic change in the difference between all of the types of modes and for all cluster sizes, with for example a RMS deviation of up to three times greater for the bending modes. The overall agreement with the reference calculations of all modes is consistently worse, in particular for the larger cluster, n = 4−6. Only the low-frequency modes of the Cs dimer seem improved by fixing the quadrupole moment. While the parametrization of the intermolecular interaction parameters is with the QMS included, the structural properties and interaction energy of the small clusters are not drastically changed with the quadrupole moment fixed (see the Supporting Information).

It is also of interest to analyze the structure of the monomers in crystal ice Ih with or without the QMS included. Table 7 presents the average internal HOH angle of each water monomer in the crystal lattice, extracted at volume V_0^{ZPE}, and compares to the experimental value of the angle for the isolated monomer and in crystal ice Ih. The experiments show a clear widening of the monomer HOH angle by about 3.5° (104.5−108.1°) going from the gas-to-crystal phase. Without the QMS, the trend is opposite, with the angle favoring lower values by about 4.5° (104.5−99.95°), where the dipole moment is high. The correct trend is captured again with the inclusion of the QMS, with the angle widening by about 2° (104.5−106.51°). The QMS correctly balances the magnitude of the dipole moment and principal quadrupole moment in the lattice, and in such a way that a widening of the angle is favored.

Table 7. Average Intramolecular HOH Angles (in Degrees) for the SCME/f Model with and without the QMS[a]

	Exp (gas)	Exp (Ih)	SCME/f	SCME/f no QMS
⟨∠HOH⟩	104.5	108.1	106.51	99.95

[a]Experimental angles for the isolate water molecule (gas) and in crystal ice Ih (Ih) are presented for comparison.

7. DISCUSSION AND CONCLUSIONS

We have presented an extension of the SCME potential function for water molecules to allow for distortion of the molecular structure. In addition to the DMS, this flexible potential function, SCME/f, includes a mapping of the QMS which has not been previously included at this level of detail to our knowledge. Potential functions that use distributed multipole expansions naturally include some of these effects as the overall molecular properties (such as multipole moments and polarizabilities) change as a function of molecular conformation. A simpler model for the quadrupole moment that has been used in both rigid and flexible point charge-based potential functions,[2,3,78−80] as well as more sophisticated polarizable models,[32−37,39,41−43] make use of the so-called M-site. We now digress in a brief comparison between the QMS model described in this work and the M-site model.

In the M-site model, the partial charge associated with the oxygen is moved off the atomic center to a position behind the oxygen and on to the bisector defined by the two OH bond vectors. The position of the M-site in the global coordinate frame is written as[114−116]

$$\boldsymbol{r}_{\mathrm{M}} = (1-\gamma)\boldsymbol{r}_{\mathrm{O}} + \frac{\gamma}{2}(\boldsymbol{r}_{\mathrm{H}_1} + \boldsymbol{r}_{\mathrm{H}_2}) \tag{41}$$

where $0 < \gamma \leq 1$. For any finite value of γ, the partial charges are re-scaled according to

$$q^{\mathrm{H}_i^{\gamma}} = \frac{q^{\mathrm{H}_i}}{1-\gamma}, \qquad q^{\mathrm{M}} = -q^{\mathrm{H}_1^{\gamma}} - q^{\mathrm{H}_2^{\gamma}} \tag{42}$$

such that the dipole moment remains unchanged in the M-site frame, and a single set of three partial charges describes both the dipole and quadrupole moment.

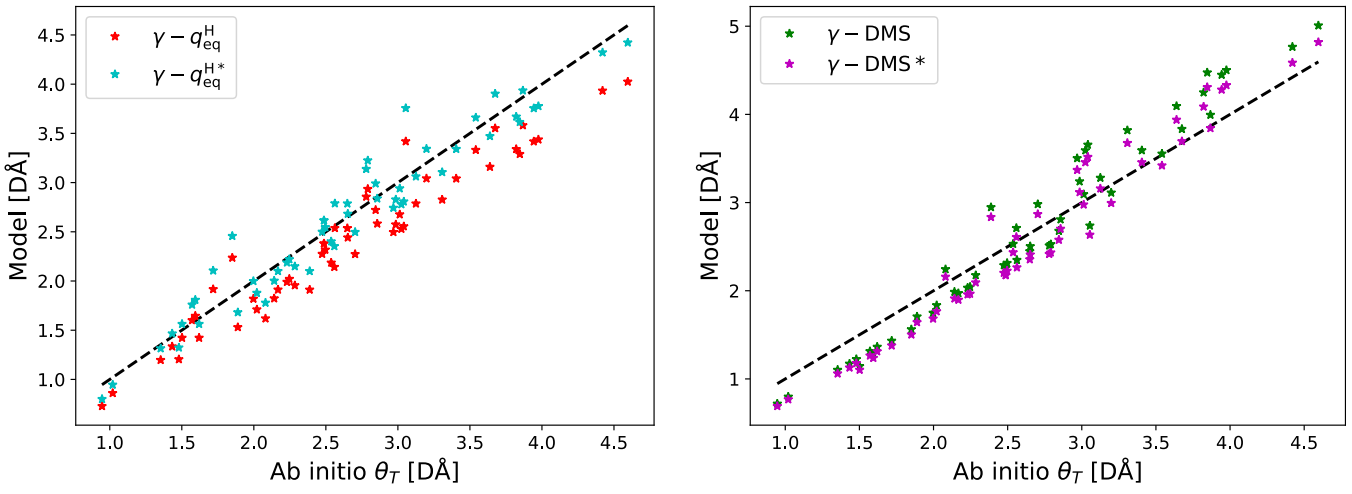

Figure 7. *M*-site models. See the Supporting Information for details on the individual models. Left: *M*-site models making use of a fixed charge ($\gamma - q_{\mathrm{eq}}^{H}$, red) corresponding to the ground-state monomer configuration or scaled charge ($\gamma - q_{\mathrm{eq}}^{H,*}$, cyan). The fixed point charge model (red) tends to underestimate the strength of the quadrupole moment over the whole range, whereas the scaling results in a change in the slope and an overall better agreement. Right: *M*-site models making use of variable DMS charges (γ − DMS, green) and scaled DMS charges (γ − DMS*, magenta). Both models tend to underestimate the strength of the quadrupole moment in region of low strength, whereas overestimate in the region of large strength. The agreement is only slightly improved with the scaled DMS model, corresponding to a shift of the *M*-site to γ = 0.3838.

https://doi.org/10.1021/acs.jctc.2c00598
J. Chem. Theory Comput. 2022, 18, 7528−7543

More importantly, a value of γ can be derived such that the Δ component in eq 33 vanishes, resulting in the compactly written moment tensor

$$\theta = \begin{bmatrix} \theta_T & 0 & 0 \\ 0 & -\theta_T & 0 \\ 0 & 0 & 0 \end{bmatrix} \tag{43}$$

This illustrates that the principal quadrupole moment component θ_T is origin independent and is the rational for placing the partial charge on the M-site and not on the oxygen center. The strength of the quadrupole moment interaction is determined by θ_T. For the ground-state PE-PES water monomer configuration used in this work, a $\gamma = 0.4071$ results in a compact tensor of the form in eq 43 (see the Supporting Information). Similar values for γ are reported in potential functions based on the M-site. While such a three site partial charge model can capture both the dipole and principal quadrupole moment for a fixed ground-state monomer configuration, the question is how the model holds up in the case of a flexible water monomer.

Using the ab initio ICE-CI quadrupole moment data, four M-site models are considered and compared and are representative of M-site models encountered in the literature. The details of the models and parameters are presented in the Supporting Information. The first two models, Figure 7 left, make use of $\gamma = 0.4071$ and a set of fixed partial charges $(\gamma - q_{eq}^{H})$—corresponding to the partial charges of the ground-state monomer configuration—or scaled ground-state charges $(\gamma - q_{eq}^{H,*})$. The scaling parameter is fit such that the model best captures θ_T over the whole range. The fixed point charge model tends to underestimate the strength of the quadrupole moment over the whole range, whereas the scaling of the charge results in a change in the slope and overall better agreement. However, in both cases, the scatter is substantial, and the RMS difference between the trace components of the quadrupole moment versus the ab initio values is >10% on average (see the Supporting Information).

In the third and fourth model, Figure 7 right, the charge are described with the DMS charge. In the third model, the optimal γ value is used (γ − DMS), and in the fourth model, the DMS charges are scaled (γ − DMS*) to best capture θ_T over the whole range. The qualitative trend is the same in both cases, with the strength of the quadrupole moment underestimated in the region of low strength, and overestimated in the region of large strength, and the overall agreement is only slightly improved with a change in the slope. Similar to the fixed charge models, the scatter is substantial, and the RMS difference is found to be ≈10%, on average.

While the simple M-site models capture the overall qualitative trend in the change of the principal quadrupole moment over a broad range of configurations, an analysis of the RMS difference of the quadrupole moment components shows that they deviate significantly for monomer configurations different than the ground-state configuration. Neither the fixed charge nor DMS charge M-site models (scaled or not) seem to better capture the principal quadrupole component over the other, and in all cases, the RMS difference is around 10% or greater. This illustrates that a three site model based on the M-site principle is not able to capture the variation of the quadrupole moment in a flexible water potential model to a good degree. The four site QMS model developed in this work, which captures the principal quadrupole moment with a mean absolute error of 0.04 DÅ, similarly has low scatter throughout the range with an average RMS difference of 1.6%, with greatest discrepancy in the region where the quadrupole moment interaction is the weakest.

Furthermore, the intermolecular interactions of the SCME/f model only depend on five parameters. The parameters have been fitted to reproduce high-level quantum chemistry calculations for the water dimer energy surface near the equilibrium geometry, and interaction energy of the lowest-lying water clusters up to and including the hexamer, as well as the properties of the Ih ice crystal—and in such a way that experimental values are reproduced to a good degree after including ZPE corrections.

The simple parameterization of the flexible model and the use of a single center for the electrostatic interactions allows for the seamless integration into our recently implemented PE-QM/MM interface.[75,76]

The calculated energy of the higher lying energy isomers of hexamer water cluster is found to be in a reasonable agreement with the results of CCSD(T) calculations in the complete basis set limit.[81] However, the inaccuracy of the potential function in the interaction energy of the pentamer and hexamer clusters (overestimation by greater than 1 kcal/mol) can be attributed to the single-site and fully isotropic modeling of the short-range interaction. We have included in the Supporting Information, a comparison with the rigid DPP2[39] model potential, which includes a distributed point model of the repulsive interaction. Furthermore, it includes charge penetration and delocalization terms. Overall, the DPP2 model captures better the total interaction energy of the hexamers, whereas the energy differences between the isomers are captured slightly better with the SCME/f potential. Most likely an extension of the repulsive interaction in SCME/f to include anisotropy would help reduce this error. In any case, SCME/f represents a significant improvement over the previously reported SCME potential function[10] and is on par with the trend predicted with the HBB2-pol[36,37] potential function, which explicitly models the N-body expansion up to the three-body terms in the interaction energy and is the predecessor of the MB-pol potential function.[41−43] However, discrepancies are present in the series of pentamer isomers, in particular the cage-like isomers. H-bonds in bonds where the distance is greater than 3 Å are found to be unstable, leading to a rearrangement of some of the SCME/f structures compared to the reference structures.

Analysis of the vibrational modes of the small water clusters reveals a substantial improvement with the QMS mapping included (as opposed to a fixed value). In particular are the intramolecular bending modes in the range 1600−1800 cm^{-1}, with maximum absolute deviation consistently less than 20 cm^{-1} with the QMS included, compared to near-CBS CCSD(T) calculations.[112,113] Importantly, including the DMS only results in the opposite trend of the intramolecular angle widening in crystal ice Ih compared to the gas phase. The inclusion of the QMS recovers the correct trend due to the balance between the magnitude of the dipole and principal quadrupole moment which are functions of the internal geometry and strongly dependent on this angle.

While the results presented here represent an important step forward in the development of a SCME model for water, there

https://doi.org/10.1021/acs.jctc.2c00598
J. Chem. Theory Comput. 2022, 18, 7528−7543

is room for improvement, and this will be addressed in future work. A natural next step to the mapping of the dipole and the quadrupole is to incorporate a mapping of the polarizability tensors. Work is ongoing to incorporate the intramolecular geometry-dependent mapping of the dipole−dipole, dipole−quadrupole, and quadrupole−quadrupole polarizability tensors by Loboda et al.[117] It has been suggested that a critical part of the H-bond OH softening lies in the correct mapping of the polarizability surface of the individual monomers.[35]

In particular, and in order to further address the overestimated H-bonded OH stretches, an improvement of the underlying water monomer potential energy surface—whose limit in terms of hydrogen dissociation is $OH^{\bullet} + H^{\bullet}$—must be made when there are neighboring water molecules such that it approaches to some degree the dissociation limit in a condensed phase which is $OH^{-} + H^{+}$. In order to capture this, one could modify the DMS and QMS charges to better represent this limit, and in a way which depends on the environment. Modifying the charge of the DMS has, for example, previously been considered in water potentials in order to capture the charge delocalization and resulting softening of the H-bond, such as in the TTM3-F model.[34]

Further improvements to this flexible SCME model that are being pursued include a more elaborate repulsive part including deviations from spherical symmetry.

■ ASSOCIATED CONTENT

Supporting Information

The Supporting Information is available free of charge at https://pubs.acs.org/doi/10.1021/acs.jctc.2c00598.

Detailed derivation of the atomic forces; comparison between the numerical and analytical forces due to the varying convergence criteria of the induced moments; parameters used for the M-site model description of the principal quadrupole moment; root-square deviation of the PS versus ICE-CI potential energy of deformed monomers; comparison between CCSD(T), SCME/f, and DPP2 total interaction and relative hexamer isomer energies; an analysis of the RMSD between ab initio versus the QMS quadrupole as well as M-site model quadrupoles with respect to geometrical variation of the monomer; binding energies and relative structural properties of the lowest-lying water clusters for the case where the quadrupole moment is set to a fixed value corresponding to the ground-state monomer configuration; and evaluation of the bulk properties from fitting the energy−volume relation—with and without ZPE corrections (PDF)

■ AUTHOR INFORMATION

Corresponding Author

Elvar Örn Jónsson − *Science Institute and Faculty of Physical Sciences, University of Iceland, 107 Reykjavík, Iceland;* orcid.org/0000-0001-6273-1237; Email: eojons@gmail.com

Authors

Soroush Rasti − *Leiden Institute of Chemistry, Gorlaeus Laboratories, Leiden University, 2300 RA Leiden, The Netherlands*

Marta Galynska − *Science Institute and Faculty of Physical Sciences, University of Iceland, 107 Reykjavík, Iceland*

Jörg Meyer − *Leiden Institute of Chemistry, Gorlaeus Laboratories, Leiden University, 2300 RA Leiden, The Netherlands;* orcid.org/0000-0003-0146-730X

Hannes Jónsson − *Science Institute and Faculty of Physical Sciences, University of Iceland, 107 Reykjavík, Iceland;* orcid.org/0000-0001-8285-5421

Complete contact information is available at: https://pubs.acs.org/10.1021/acs.jctc.2c00598

Notes

The authors declare no competing financial interest.

■ ACKNOWLEDGMENTS

This work was supported by the University of Iceland Research Fund and the Icelandic Research Fund, grants no. 174082-051, 141080-051, and 207283-051. M.G. acknowledges postdoctoral fellowship from the University of Iceland Research Fund and thanks Ragnar Björnsson for helpful discussions and guidance in the electronic structure calculations of the H_2O molecule. J.M. acknowledges support from The Netherlands Organization for Scientific Research (NWO) under Vidi grant no. 723.014.009. Figures showing water molecules were drawn with open-source software Inkscape[118] (licence GPL).

■ ADDITIONAL NOTE

[a]Throughout this work, we make use of Einstein notation, that is, Cartesian vector spaces are indexed with Greek letters, $\alpha = \beta = \cdots = \nu \in \{x, y, z\}$, and repeated Greek indices are to be summed over.

■ REFERENCES

(1) Jorgensen, W. L.; Chandrasekhar, J.; Madura, J. D.; Impey, R. W.; Klein, M. L. Comparison of simple potential functions for simulating liquid water. *J. Chem. Phys.* **1983**, *79*, 926−935.

(2) Jorgensen, W. L. Quantum and statistical mechanical studies of liquids. 10. Transferable intermolecular potential functions for water, alcohols, and ethers. Application to liquid water. *J. Am. Chem. Soc.* **1981**, *103*, 335−340.

(3) Horn, H. W.; Swope, W. C.; Pitera, J. W.; Madura, J. D.; Dick, T. J.; Hura, G. L.; Head-Gordon, T. Development of an Improved Four-Site Water Model for Biomolecular Simulations: TIP4P-Ew. *J. Chem. Phys.* **2004**, *120*, 9665.

(4) Zielkiewicz, J. Structural properties of water: Comparison of the SPC, SPCE, TIP4P, and TIP5P models of water. *J. Chem. Phys.* **2005**, *123*, 104501.

(5) Park, K.; Lin, W.; Paesani, F. A Refined MS-EVB Model for Proton Transport in Aqueous Environments. *J. Phys. Chem. B* **2012**, *116*, 343−352.

(6) Habershon, S.; Markland, T. E.; Manolopoulos, D. E. Competing quantum effects in the dynamics of a flexible water model. *J. Chem. Phys.* **2009**, *131*, 024501.

(7) Batista, E. R.; Xantheas, S. S.; Jónsson, H. Molecular Multipole Moments of Water Molecules in Ice Ih. *J. Chem. Phys.* **1998**, *109*, 4546.

(8) Batista, E. R.; Xantheas, S. S.; Jónsson, H. Electric fields in ice and near water clusters. *J. Chem. Phys.* **2000**, *112*, 3285.

(9) Batista, E.*Development of a New Water−Water Interaction Potential and Applications to Molecular Processes in Ice*; University of Washington, 1999.

(10) Wikfeldt, K. T.; Batista, E. R.; Vila, F. D.; Jónsson, H. A transferable H2O interaction potential based on a single center multipole expansion: SCME. *Phys. Chem. Chem. Phys.* **2013**, *15*, 16542.

(11) Smirnov, I. V.; Golovin, A. V.; Chatziefthimiou, S. D.; Stepanova, A. V.; Peng, Y.; Zolotareva, O. I.; Belogurov, A. A.;

Kurkova, I. N.; Ponomarenko, N. A.; Wilmanns, M.; Blackburn, G. M.; Gabibov, A. G.; Lerner, R. A. Robotic QM/MM-driven maturation of antibody combining sites. *Sci. Adv.* **2016**, *2*, No. e1501695.
(12) Barends, T. R. M.; Foucar, L.; Ardevol, A.; Nass, K.; Aquila, A.; Botha, S.; Doak, R. B.; Falahati, K.; Hartmann, E.; Hilpert, M.; Heinz, M.; Hoffmann, M. C.; Köfinger, J.; Koglin, J. E.; Kovacsova, G.; Liang, M.; Milathianaki, D.; Lemke, H. T.; Reinstein, J.; Roome, C. M.; Shoeman, R. L.; Williams, G. J.; Burghardt, I.; Hummer, G.; Boutet, S.; Schlichting, I. Direct observation of ultrafast collective motions in CO myoglobin upon ligand dissociation. *Science* **2015**, *350*, 445−450.
(13) Senn, H. M.; Thiel, W. QM/MM methods for biomolecular systems. *Angew. Chem., Int. Ed. Engl.* **2009**, *48*, 1198−1229.
(14) Senthilkumar, K.; Mujika, J. I.; Ranaghan, K. E.; Manby, F. R.; Mulholland, A. J.; Harvey, J. N. Analysis of polarization in QM/MM modelling of biologically relevant hydrogen bonds. *J. R. Soc. Interface* **2008**, *5*, 207−216.
(15) Warshel, A.; Sharma, P. K.; Kato, M.; Xiang, Y.; Liu, H.; Olsson, M. H. M. Electrostatic basis for enzyme catalysis. *Chem. Rev.* **2006**, *106*, 3210−3235.
(16) Zheng, F.; Xue, L.; Hou, S.; Liu, J.; Zhan, M.; Yang, W.; Zhan, C.-G. A highly efficient cocaine-detoxifying enzyme obtained by computational design. *Nat. Commun.* **2014**, *5*, 3457.
(17) Knorr, J.; Sokkar, P.; Schott, S.; Costa, P.; Thiel, W.; Sander, W.; Sanchez-Garcia, E.; Nuernberger, P. Competitive solvent-molecule interactions govern primary processes of diphenylcarbene in solvent mixtures. *Nat. Commun.* **2016**, *7*, 12968.
(18) Pham, V.-T.; Penfold, T. J.; van der Veen, R. M.; Lima, F.; El Nahhas, A. E.; Johnson, S. L.; Beaud, P.; Abela, R.; Bressler, C.; Tavernelli, I.; Milne, C. J.; Chergui, M. Probing the Transition from Hydrophilic to Hydrophobic Solvation with Atomic Scale Resolution. *J. Am. Chem. Soc.* **2011**, *133*, 12740−12748.
(19) Dohn, A. O.; Jónsson, E. O.; Kjær, K. S.; van Driel, B.; Jacobsen, T.; Nielsen, M. M.; Jacobsen, K. W.; Henriksen, N. E.; Møller, K. B. Direct Dynamics Studies of a Binuclear Metal Complex in Solution: The Interplay Between Vibrational Relaxation, Coherence, and Solvent Effects. *J. Phys. Chem. Lett.* **2014**, *5*, 2414−2418.
(20) Dohn, A. O.; Kjær, K. S.; Harlang, T. B.; Canton, S. E.; Nielsen, M. M.; Møller, K. B. Electron Transfer and Solvent-Mediated Electronic Localization in Molecular Photocatalysis. *Inorg. Chem.* **2016**, *55*, 10637−10644.
(21) Levi, G.; Pápai, M.; Henriksen, N. E.; Dohn, A. O.; Møller, K. B. Solution Structure and Ultrafast Vibrational Relaxation of the PtPOP Complex Revealed by ΔSCF-QM/MM Direct Dynamics Simulations. *J. Chem. Phys. C* **2018**, *122*, 7100−7119.
(22) Dohn, A. O.; Selli, D.; Fazio, G.; Ferraro, L.; Mortensen, J.; Civalleri, B.; Valentin, C. D. Interfacing CRYSTAL/AMBER to Optimize QM/MM Lennard−Jones Parameters for Water and to Study Solvation of TiO2 Nanoparticles. *Molecules* **2018**, *23*, 2958.
(23) Zhang, Y.-J.; Khorshidi, A.; Kastlunger, G.; Peterson, A. A. The potential for machine learning in hybrid QM/MM calculations. *J. Chem. Phys.* **2018**, *148*, 241740.
(24) Lin, H.; Truhlar, D. G. QM/MM: what have we learned, where are we, and where do we go from here? *Theor. Chem. Acc.* **2006**, *117*, 185.
(25) Pezeshki, S.; Lin, H. Recent developments in QM/MM methods towards open-boundary multi-scale simulations. *Mol. Simulat.* **2015**, *41*, 168−189.
(26) Sneskov, K.; Schwabe, T.; Christiansen, O.; Kongsted, J. Scrutinizing the effects of polarization in QM/MM excited state calculations. *Phys. Chem. Chem. Phys.* **2011**, *13*, 18551−18560.
(27) Morzan, U. N.; Alonso de Armiño, D. J. A.; Foglia, N. O.; Ramírez, F.; González Lebrero, M. C. G.; Scherlis, D. A.; Estrin, D. A. Spectroscopy in Complex Environments from QM-MM Simulations. *Chem. Rev.* **2018**, *118*, 4071−4113.
(28) Warshel, A.; Levitt, M. Theoretical studies of enzymic reactions: Dielectric, electrostatic and steric stabilization of the carbonium ion in the reaction of lysozyme. *J. Mol. Biol.* **1976**, *103*, 227−249.
(29) Cisneros, G. A.; Wikfeldt, K. T.; Ojamäe, L.; Lu, J.; Xu, Y.; Torabifard, H.; Bartók, A. P.; Csányi, G.; Molinero, V.; Paesani, F. Modeling Molecular Interactions in Water: From Pairwise to Many-Body Potential Energy Functions. *Chem. Rev.* **2016**, *116*, 7501−7528.
(30) Yu, H.; van Gunsteren, W. F. Accounting for polarization in molecular simulation. *Comput. Phys. Commun.* **2005**, *172*, 69−85.
(31) Lopes, P. E.; Roux, B.; MacKerell, A. D. Molecular modeling and dynamics studies with explicit inclusion of electronic polarizability: theory and applications. *Theor. Chem. Acc.* **2009**, *124*, 11−28.
(32) Burnham, C. J.; Xantheas, S. S. Development of transferable interaction models for water. I. Prominent features of the water dimer potential energy surface. *J. Chem. Phys.* **2002**, *116*, 1479−1492.
(33) Fanourgakis, G. S.; Xantheas, S. S. The Flexible, Polarizable, Thole-Type Interaction Potential for Water (TTM2-F) Revisited. *J. Phys. Chem. A* **2006**, *110*, 4100−4106.
(34) Fanourgakis, G. S.; Xantheas, S. S. Development of transferable interaction potentials for water. V. Extension of the flexible, polarizable, Thole-type model potential (TTM3-F, v. 3.0) to describe the vibrational spectra of water clusters and liquid water. *J. Chem. Phys.* **2008**, *128*, 074506.
(35) Burnham, C.; Anick, D.; Mankoo, P.; Reiter, G. The vibrational proton potential in bulk liquid water and ice. *J. Chem. Phys.* **2008**, *128*, 154519.
(36) Medders, G. R.; Babin, V.; Paesani, F. A critical assessment of two-body and three-body interactions in water. *J. Chem. Theory Comput.* **2013**, *9*, 1103−1114.
(37) Babin, V.; Medders, G. R.; Paesani, F. Toward a universal water model: First principles simulations from the dimer to the liquid phase. *J. Phys. Chem. Lett.* **2012**, *3*, 3765−3769.
(38) Millot, C.; Soetens, J.-C.; Martins Costa, M. T. C.; Hodges, M. P.; Stone, A. J. Revised Anisotropic Site Potentials for the Water Dimer and Calculated Properties. *J. Phys. Chem. A* **1998**, *102*, 754−770.
(39) Kumar, R.; Wang, F.-F.; Jenness, G. R.; Jordan, K. D. A second generation distributed point polarizable water model. *J. Chem. Phys.* **2010**, *132*, 014309.
(40) Gilmore, R. A. J.; Dove, M. T.; Misquitta, A. J. First-Principles Many-Body Nonadditive Polarization Energies from Monomer and Dimer Calculations Only: A Case Study on Water. *J. Chem. Theory Comput.* **2020**, *16*, 224−242 PMID: 31769980.
(41) Babin, V.; Leforestier, C.; Paesani, F. Development of a "first principles" water potential with flexible monomers: Dimer potential energy surface, VRT spectrum, and second virial coefficient. *J. Chem. Theory Comput.* **2013**, *9*, 5395−5403.
(42) Babin, V.; Medders, G. R.; Paesani, F. Development of a "first principles" water potential with flexible monomers. II: Trimer potential energy surface, third virial coefficient, and small clusters. *J. Chem. Theory Comput.* **2014**, *10*, 1599−1607.
(43) Medders, G. R.; Babin, V.; Paesani, F. Development of a "First-Principles" Water Potential with Flexible Monomers. III. Liquid Phase Properties. *J. Chem. Theory Comput.* **2014**, *10*, 2906−2910.
(44) Thompson, M. A.; Schenter, G. K. Excited states of the bacteriochlorophyll b dimer of Rhodopseudomonas viridis: a QM/MM study of the photosynthetic reaction center that includes MM polarization. *J. Phys. Chem.* **1995**, *99*, 6374−6386.
(45) Thompson, M. A. QM/MMpol: A Consistent Model for Solute/Solvent Polarization. Application to the Aqueous Solvation and Spectroscopy of Formaldehyde, Acetaldehyde, and Acetone. *J. Phys. Chem.* **1996**, *100*, 14492−14507.
(46) Bryce, R. A.; Buesnel, R.; Hillier, I. H.; Burton, N. A. A solvation model using a hybrid quantum mechanical/molecular mechanical potential with fluctuating solvent charges. *Chem. Phys. Lett.* **1997**, *279*, 367−371.
(47) Lipparini, F.; Barone, V. Polarizable force fields and polarizable continuum model: a fluctuating charges/PCM approach. 1. theory and implementation. *J. Chem. Theory Comput.* **2011**, *7*, 3711−3724.
(48) Boulanger, E.; Thiel, W. Solvent Boundary Potentials for Hybrid QM/MM Computations Using Classical Drude Oscillators: A

https://doi.org/10.1021/acs.jctc.2c00598
J. Chem. Theory Comput. 2022, 18, 7528−7543

Fully Polarizable Model. *J. Chem. Theory Comput.* **2012**, *8*, 4527−4538.
(49) Lu, Z.; Zhang, Y. Interfacing ab initio quantum mechanical method with classical Drude osillator polarizable model for molecular dynamics simulation of chemical reactions. *J. Chem. Theory Comput.* **2008**, *4*, 1237−1248.
(50) Thellamurege, N. M.; Si, D.; Cui, F.; Zhu, H.; Lai, R.; Li, H. QuanPol: A full spectrum and seamless QM/MM program. *J. Comput. Chem.* **2013**, *34*, 2816−2833.
(51) Kratz, E. G.; Walker, A. R.; Lagardère, L.; Lipparini, F.; Piquemal, J.-P.; Andrés Cisneros, G. LICHEM: A QM/MM program for simulations with multipolar and polarizable force fields. *J. Comput. Chem.* **2016**, *37*, 1019−1029.
(52) Dziedzic, J.; Mao, Y.; Shao, Y.; Ponder, J.; Head-Gordon, T.; Head-Gordon, M.; Skylaris, C.-K. TINKTEP: A fully self-consistent, mutually polarizable QM/MM approach based on the AMOEBA force field. *J. Chem. Phys.* **2016**, *145*, 124106.
(53) Gomes, A. S. P.; Jacob, C. R. Quantum-chemical embedding methods for treating local electronic excitations in complex chemical systems. *Annu. Rep. Prog. Chem., Sect. C: Phys. Chem.* **2012**, *108*, 222−277.
(54) Söderhjelm, P.; Husberg, C.; Strambi, A.; Olivucci, M.; Ryde, U. Protein influence on electronic spectra modeled by multipoles and polarizabilities. *J. Chem. Theory Comput.* **2009**, *5*, 649−658.
(55) Sneskov, K.; Schwabe, T.; Kongsted, J.; Christiansen, O. The polarizable embedding coupled cluster method. *J. Chem. Phys.* **2011**, *134*, 104108.
(56) Caprasecca, S.; Jurinovich, S.; Viani, L.; Curutchet, C.; Mennucci, B. Geometry optimization in polarizable QM/MM models: the induced dipole formulation. *J. Chem. Theory Comput.* **2014**, *10*, 1588−1598.
(57) Kongsted, J.; Osted, A.; Mikkelsen, K. V.; Christiansen, O. The QM/MM approach for wavefunctions, energies and response functions within self-consistent field and coupled cluster theories. *Mol. Phys.* **2002**, *100*, 1813−1828.
(58) Zeng, Q.; Liang, W. Analytic energy gradient of excited electronic state within TDDFT/MMpol framework: Benchmark tests and parallel implementation. *J. Chem. Phys.* **2015**, *143*, 134104.
(59) Loco, D.; Polack, É.; Caprasecca, S.; Lagardère, L.; Lipparini, F.; Piquemal, J.-P.; Mennucci, B. A QM/MM Approach Using the AMOEBA Polarizable Embedding: From Ground State Energies to Electronic Excitations. *J. Chem. Theor. Comput.* **2016**, *12*, 3654−3661.
(60) Loco, D.; Lagardère, L.; Caprasecca, S.; Lipparini, F.; Mennucci, B.; Piquemal, J.-P. Hybrid QM/MM molecular dynamics with AMOEBA polarizable embedding. *J. Chem. Theory Comput.* **2017**, *13*, 4025−4033.
(61) Jensen, L.; van Duijnen, P. T.; Snijders, J. G. A discrete solvent reaction field model for calculating molecular linear response properties in solution. *J. Chem. Phys.* **2003**, *119*, 3800−3809.
(62) Steindal, A. H.; Ruud, K.; Frediani, L.; Aidas, K.; Kongsted, J. Excitation Energies in Solution: The Fully Polarizable QM/MM/PCM Method. *J. Phys. Chem. B* **2011**, *115*, 3027−3037.
(63) Nielsen, C. B.; Christiansen, O.; Mikkelsen, K. V.; Kongsted, J. Density functional self-consistent quantum mechanics/molecular mechanics theory for linear and nonlinear molecular properties: Applications to solvated water and formaldehyde. *J. Chem. Phys.* **2007**, *126*, 154112.
(64) Olsen, J. M.; Aidas, K.; Kongsted, J. Excited states in solution through polarizable embedding. *J. Chem. Theory Comput.* **2010**, *6*, 3721−3734.
(65) Lipparini, F.; Cappelli, C.; Barone, V. Linear response theory and electronic transition energies for a fully polarizable QM/classical Hamiltonian. *J. Chem. Theory Comput.* **2012**, *8*, 4153−4165.
(66) Curutchet, C.; Muñoz-Losa, A.; Monti, S.; Kongsted, J.; Scholes, G. D.; Mennucci, B. Electronic Energy Transfer in Condensed Phase Studied by a Polarizable QM/MM Model. *J. Chem. Theory Comput.* **2009**, *5*, 1838−1848.
(67) List, N. H.; Olsen, J. M. H.; Kongsted, J. Excited states in large molecular systems through polarizable embedding. *Phys. Chem. Chem. Phys.* **2016**, *18*, 20234−20250.
(68) Schwörer, M.; Breitenfeld, B.; Tröster, P.; Bauer, S.; Lorenzen, K.; Tavan, P.; Mathias, G. Coupling density functional theory to polarizable force fields for efficient and accurate Hamiltonian molecular dynamics simulations. *J. Chem. Phys.* **2013**, *138*, 244103.
(69) Curutchet, C.; Muñoz-Losa, A.; Monti, S.; Kongsted, J.; Scholes, G. D.; Mennucci, B. Electronic Energy Transfer in Condensed Phase Studied by a Polarizable QM/MM Model. *J. Chem. Theory Comput.* **2009**, *5*, 1838−1848.
(70) Visscher, K.; Swope, W.; Geerke, D. A QM/MM Derived Polarizable Water Model for Molecular Simulation. *Molecules* **2018**, *23*, 3131.
(71) Hršak, D.; Olsen, J. M. H.; Kongsted, J. Polarizable Density Embedding Coupled Cluster Method. *J. Chem. Theory Comput.* **2018**, *14*, 1351.
(72) Menger, M. F. S. J.; Caprasecca, S.; Mennucci, B. Excited-State Gradients in Polarizable QM/MM Models: An Induced Dipole Formulation. *J. Chem. Theory Comput.* **2017**, *13*, 3778−3786.
(73) Mao, Y.; Shao, Y.; Dziedzic, J.; Skylaris, C.-K.; Head-Gordon, T.; Head-Gordon, M. Performance of the AMOEBA Water Model in the Vicinity of QM Solutes: A Diagnosis Using Energy Decomposition Analysis. *J. Chem. Theory Comput.* **2017**, *13*, 1963−1979.
(74) Dziedzic, J.; Head-Gordon, T.; Head-Gordon, M.; Skylaris, C.-K. Mutually polarizable QM/MM model with in situ optimized localized basis functions. *J. Chem. Phys.* **2019**, *150*, 074103.
(75) Jónsson, E. O.; Dohn, A. O.; Jónsson, H. Polarizable Embedding with a Transferable H2O Potential Function I: Formulation and Tests on Dimer. *J. Chem. Theory Comput.* **2019**, *15*, 6562−6577.
(76) Dohn, A. O.; Jónsson, E. O.; Jónsson, H. Polarizable Embedding with a Transferable H2O Potential Function II: Application to (H2O)n Clusters and Liquid Water. *J. Chem. Theory Comput.* **2019**, *15*, 6578−6587.
(77) Partridge, H.; Schwenke, D. W. The determination of an accurate isotope dependent potential energy surface for water from extensive ab initio calculations and experimental data. *J. Chem. Phys.* **1997**, *106*, 4618−4639.
(78) Habershon, S.; Markland, T. E.; Manolopoulos, D. E. Competing quantum effects in the dynamics of a flexible water model. *J. Chem. Phys.* **2009**, *131*, 024501.
(79) Abascal, J.; Sanz, E.; García Fernández, R.; Vega, C. A potential model for the study of ices and amorphous water: TIP4P/Ice. *J. Chem. Phys.* **2005**, *122*, 234511.
(80) Abascal, J. L.; Vega, C. A general purpose model for the condensed phases of water: TIP4P/2005. *J. Chem. Phys.* **2005**, *123*, 234505.
(81) Bates, D. M.; Tschumper, G. S. CCSD(T) Complete Basis Set Limit Relative Energies for Low-Lying Water Hexamer Structures. *J. Phys. Chem. A* **2009**, *113*, 3555−3559.
(82) Temelso, B.; Archer, K. A.; Shields, G. C. Benchmark Structures and Binding Energies of Small Water Clusters with Anharmonicity Corrections. *J. Phys. Chem. A* **2011**, *115*, 12034−12046.
(83) Lipparini, F.; Lagardère, L.; Stamm, B.; Cancès, E.; Schnieders, M.; Ren, P.; Maday, Y.; Piquemal, J.-P. Scalable Evaluation of Polarization Energy and Associated Forces in Polarizable Molecular Dynamics: I. Toward Massively Parallel Direct Space Computations. *J. Chem. Theory Comput.* **2014**, *10*, 1638−1651.
(84) Stone, A.*The Theory of Intermolecular Forces*; OUP Oxford, 2013.
(85) Thole, B. Molecular polarizabilities calculated with a modified dipole interaction. *Chem. Phys.* **1981**, *59*, 341−350.
(86) Masia, M.; Probst, M.; Rey, R. On the performance of molecular polarization methods. II. Water and carbon tetrachloride close to a cation. *J. Chem. Phys.* **2005**, *123*, 164505.
(87) Masia, M.; Probst, M.; Rey, R. Polarization damping in halide-water dimers. *Chem. Phys. Lett.* **2006**, *420*, 267−270.

(88) Burnham, C. J.; Li, J.; Xantheas, S. S.; Leslie, M. The parametrization of a Thole-type all-atom polarizable water model from first principles and its application to the study of water clusters (n=2-21) and the phonon spectrum of ice Ih. *J. Chem. Phys.* **1999**, *110*, 4566−4581.
(89) Stone, A. J. Electrostatic damping functions and the penetration energy. *J. Phys. Chem. A* **2011**, *115*, 7017−7027.
(90) Sala, J.; Guàrdia, E.; Masia, M. The polarizable point dipoles method with electrostatic damping: Implementation on a model system. *J. Chem. Phys.* **2010**, *133*, 234101.
(91) Wikfeldt, K. T.; Batista, E. R.; Vila, F. D.; Jónsson, H. A transferable H2O interaction potential based on a single center multipole expansion: SCME. *Phys. Chem. Chem. Phys.* **2013**, *15*, 16542.
(92) Wormer, P. E.; Hettema, H. Many-body perturbation theory of frequency-dependent polarizabilities and van der Waals coefficients: Application to H2O-H2O and Ar-NH3. *J. Chem. Phys.* **1992**, *97*, 5592−5606.
(93) Tang, K.; Toennies, J. P. An improved simple model for the van der Waals potential based on universal damping functions for the dispersion coefficients. *J. Chem. Phys.* **1984**, *80*, 3726−3741.
(94) Rodrigues, O. Des lois géometriques qui regissent les déplacements d' un systéme solide dans l' espace, et de la variation des coordonnées provenant de ces déplacement considérées indépendant des causes qui peuvent les produire. *J. Math. Pure Appl.* **1840**, *5*, 380−440.
(95) Neese, F. The ORCA program system. *Wiley Interdiscip. Rev.: Comput. Mol. Sci.* **2012**, *2*, 73−78.
(96) Neese, F. Software update: the ORCA program system, version 4.0. *Wiley Interdiscip. Rev.: Comput. Mol. Sci.* **2018**, *8*, No. e1327.
(97) Huron, B.; Malrieu, J.; Rancurel, P. Iterative perturbation calculations of ground and excited state energies from multiconfigurational zeroth-order wavefunctions. *J. Chem. Phys.* **1973**, *58*, 5745−5759.
(98) Virtanen, P.; Gommers, R.; Oliphant, T. E.; Haberland, M.; Reddy, T.; Cournapeau, D.; Burovski, E.; Peterson, P.; Weckesser, W.; Bright, J.; van der Walt, S. J.; Brett, M.; Wilson, J.; Millman, K.; Mayorov, N.; Nelson, A. R. J.; Jones, E.; Kern, R.; Larson, E.; Carey, C.; Polat, İ.; Feng, Y.; Moore, E. W.; VanderPlas, J.; Laxalde, D.; Perktold, J.; Cimrman, R.; Henriksen, I.; Quintero, E. A.; Harris, C. R.; Archibald, A. M.; Ribeiro, A. H.; Pedregosa, F.; van Mulbregt, P.; Vijaykumar, S.; Bardelli, A. P.; Rothberg, A.; Hilboll, A.; Kloeckner, A.; Scopatz, A.; Lee, A.; Rokem, A.; Woods, C. N.; Fulton, C.; Masson, C.; Häggström, C.; Fitzgerald, C.; Nicholson, D. A.; Hagen, D. R.; Pasechnik, D. V.; Olivetti, E.; Martin, E.; Wieser, E.; Silva, F.; Lenders, F.; Wilhelm, F.; Young, G.; Price, G. A.; Ingold, G.-L.; Allen, G. E.; Lee, G. R.; Audren, H.; Probst, I.; Dietrich, J. P.; Silterra, J.; Webber, J. T.; Slavič, J.; Nothman, J.; Buchner, J.; Kulick, J.; Schönberger, J. L.; de Miranda Cardoso, J. V.; Reimer, J.; Harrington, J.; Rodríguez, J. L. C.; Nunez-Iglesias, J.; Kuczynski, J.; Tritz, K.; Thoma, M.; Newville, M.; Kümmerer, M.; Bolingbroke, M.; Tartre, M.; Pak, M.; Smith, N. J.; Nowaczyk, N.; Shebanov, N.; Pavlyk, O.; Brodtkorb, P. A.; Lee, P.; McGibbon, R. T.; Feldbauer, R.; Lewis, S.; Tygier, S.; Sievert, S.; Vigna, S.; Peterson, S.; More, S.; Pudlik, T.; Oshima, T.; Pingel, T. J.; Robitaille, T. P.; Spura, T.; Jones, T. R.; Cera, T.; Leslie, T.; Zito, T.; Krauss, T.; Upadhyay, U.; Halchenko, Y. O.; Vázquez-Baeza, Y. SciPy 1.0: Fundamental Algorithms for Scientific Computing in Python. *Nat. Methods* **2020**, *17*, 261−272.
(99) SCME. https://gitlab.com/theochem-ui/ (Accessed October 2022).
(100) Bahn, S. R.; Jacobsen, K. W. An object-oriented scripting interface to a legacy electronic structure code. *Comput. Sci. Eng.* **2002**, *4*, 56.
(101) Larsen, A. H.; Mortensen, J. J.; Blomqvist, J.; Castelli, I. E.; Christensen, R.; Dułak, M.; Friis, J.; Groves, M. N.; Hammer, B.; Hargus, C.; Hermes, E. D.; Jennings, P. C.; Jensen, P. B.; Kermode, J.; Kitchin, J. R.; Kolsbjerg, E. L.; Kubal, J.; Kaasbjerg, K.; Lysgaard, S.; Maronsson, J. B.; Maxson, T.; Olsen, T.; Pastewka, L.; Peterson, A.; Rostgaard, C.; Schiøtz, J.; Schütt, O.; Strange, M.; Thygesen, K. S.; Vegge, T.; Vilhelmsen, L.; Walter, M.; Zeng, Z.; Jacobsen, K. W. The atomic simulation environment—a Python library for working with atoms. *J. Phys. Condens. Matter* **2017**, *29*, 273002.
(102) Whalley, E. The difference in the intermolecular forces of H2O and D2O. *Trans. Faraday Soc.* **1957**, *53*, 1578.
(103) Whalley, E. Zero-Point Energy: A Contribution to Intermolecular Forces. *Trans. Faraday Soc.* **1958**, *54*, 1613.
(104) Whalley, E. Energies of the Phases of Ice at Zero Temperature and Pressure. *J. Chem. Phys.* **1984**, *81*, 4087−4092.
(105) Rasti, S.; Meyer, J. Importance of zero-point energy for crystalline ice phases: A comparison of force fields and density functional theory. *J. Chem. Phys.* **2019**, *150*, 234504.
(106) Parlinski, K.; Li, Z. Q.; Kawazoe, Y. First-Principles Determination of the Soft Mode in CubicZrO2. *Phys. Rev. Lett.* **1997**, *78*, 4063−4066.
(107) Togo, A.; Tanaka, I. First Principles Phonon Calculations in Materials Science. *Scripta Mater.* **2015**, *108*, 1−5.
(108) Vinet, P.; Smith, J. R.; Ferrante, J.; Rose, J. H. Temperature Effects on the Universal Equation of State of Solids. *Phys. Rev. B: Condens. Matter Mater. Phys.* **1987**, *35*, 1945−1953.
(109) Röttger, K.; Endriss, A.; Ihringer, J.; Doyle, S.; Kuhs, W. F. Lattice constants and thermal expansion of H2O and D2O ice Ih between 10 and 265 K. *Acta Crystallogr., Sect. B: Struct. Sci.* **1994**, *50*, 644−648.
(110) Hobbs, P. V.*Ice Physics*; Oxford University Press, 2010.
(111) Kabsch, W. A solution for the best rotation to relate two sets of vectors. *Acta Crystallogr., Sect. A: Cryst. Phys., Diffr., Theor. Gen. Crystallogr.* **1976**, *32*, 922−923.
(112) Howard, J. C.; Gray, J. L.; Hardwick, A. J.; Nguyen, L. T.; Tschumper, G. S. Getting down to the Fundamentals of Hydrogen Bonding: Anharmonic Vibrational Frequencies of (HF)2 and (H2O)2 from Ab Initio Electronic Structure Computations. *J. Chem. Theory Comput.* **2014**, *10*, 5426−5435.
(113) Howard, J. C.; Tschumper, G. S. Benchmark Structures and Harmonic Vibrational Frequencies Near the CCSD(T) Complete Basis Set Limit for Small Water Clusters: (H2O)n = 2, 3, 4, 5, 6. *J. Chem. Theory Comput.* **2015**, *11*, 2126−2136.
(114) Reimers, J.; Watts, R.; Klein, M. Intermolecular potential functions and the properties of water. *Chem. Phys.* **1982**, *64*, 95−114.
(115) Reimers, J.; Watts, R. The structure and vibrational spectra of small clusters of water molecules. *Chem. Phys.* **1984**, *85*, 83−112.
(116) Suhm, M. A.; Watts, R. O. Parameterized dipole moment function for the water molecule. *Mol. Phys.* **1991**, *73*, 463−469.
(117) Loboda, O.; Ingrosso, F.; Ruiz-López, M. F.; Reis, H.; Millot, C. Dipole and quadrupole polarizabilities of the water molecule as a function of geometry. *J. Comput. Chem.* **2016**, *37*, 2125−2132.
(118) Harrington, B.; et al.*Inkscape*. http://www.inkscape.org/, 2004−2005.
(119) Bjerrum, N. Structure and Properties of Ice. *Science* **1952**, *115*, 385−390.

https://doi.org/10.1021/acs.jctc.2c00598
J. Chem. Theory Comput. 2022, 18, 7528−7543